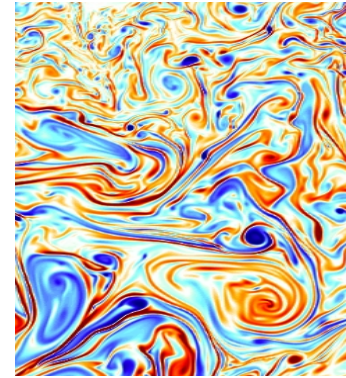
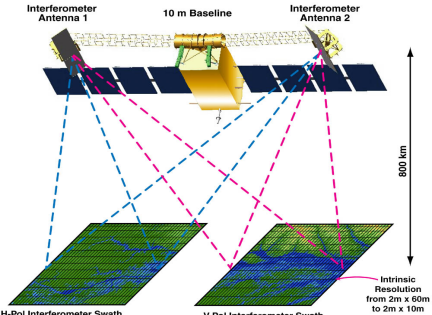


”Ocean Turbulence from SPACE”

(III) – Satellite Altimetry (a)

Patrice Klein (Caltech/JPL/Ifremer)



Satellite altimetry:

- 1 - Major breakthroughs and existing limitations.
- 2 - Expectations from future altimeter missions and need for a better dynamical framework.

Some relevant papers:

- Morrow R. and P.Y. Le Traon (2012): Recent advances in observing mesoscale ocean dynamics with satellite altimetry. *Adv. in Space Res.*
- P.Y. Le Traon (2013): From satellite altimetry to Argo and operational oceanography. *Oc. Sci.*
- Chelton et al. (2011): Global observations of nonlinear eddies. *Prog. Ocean.* (50p)
- Y. Xu and L.L. Fu (2012): The effects of altimeter instrument noise on the estimation of the wavenumber spectrum of Sea Surface Height. *J.P.O.*
- Zhai et al. (2008): On the seasonal variability of eddy kinetic energy in the Gulf Stream region. *GRL*.
- Dong et al. (2014): Global heat and salt transports by eddy movements. *Nat. Comm.*
- Zhang et al. (2014): Oceanic mass transport by oceanic eddies. *Science*
- Fu L.L. and R. Ferrari (2008): Observing oceanic submesoscale processes from space. *EOS*.

Textbook: S. Martin (2014) « An introduction to Ocean Remote Sensing » C.U.P.

Satellite radar altimetry: some principles (from S. Martin, 2014)

The radar altimeter transmits short pulses of energy toward the ocean surface.

The return yields information on the variability of sea surface height (SSH).

Specifically, the time difference between the transmitted and received signals measures the distance between the satellite and the sea surface.

If

- (1) the satellite orbit is precisely determined and the distance is corrected for the impact of the
 - (2) ionospheric factors,
 - (3) atmospheric water vapor and liquid water cloud, and for
 - (4) topography impact on ocean surface (geoid) ,
- these observations measure, to an accuracy of 2-3 cm, the changes in SSH associated with tides and geostrophic motions.



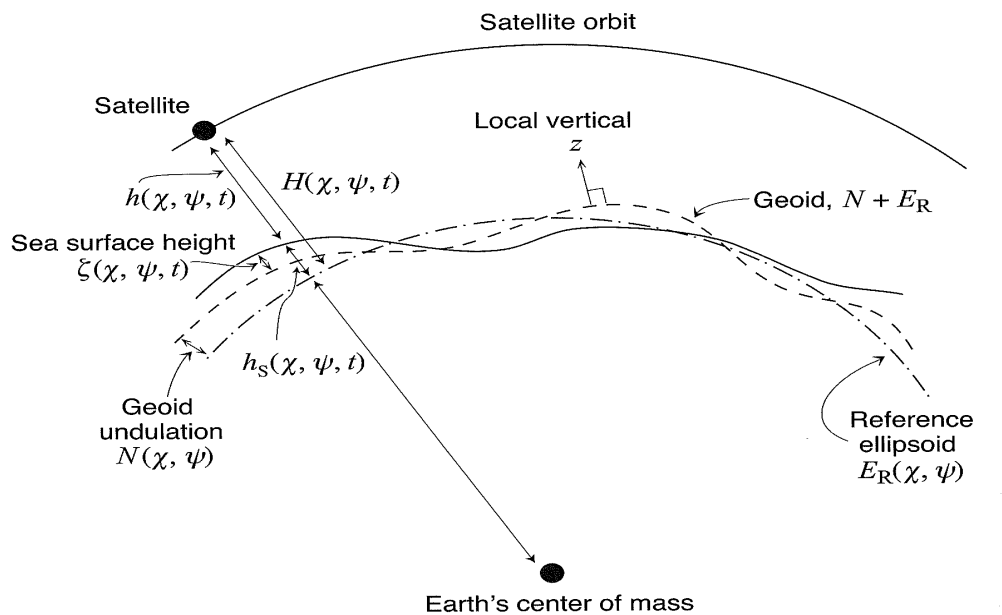
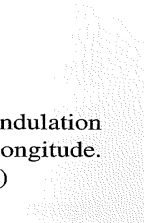


Fig. 12.1. The altimeter geometry showing the satellite orbit, the reference ellipsoid, geoid undulation and height of the sea surface above the Earth's center of mass, where χ is latitude and ψ is longitude. See the text for further description. (Adapted from Figure 3, Wunsch and Stammer (1998).)



The altimeter measures the height h . h is affected by the ionospheric free electrons (**2 altimeters**), the water vapor and the cloud liquid water (**microwave radiometer**).

H is the height of the satellite above the ellipsoid. This requires to determine the precise position of the satellite (in 3D). Three methods: **GPS, DORIS, Laser retroreflector**

N is the geoid. This is the steady-state sea level (in the absence of external forces, winds tides, eddies) produced by the uneven distribution of the Earth's mass.

$\zeta = H - h - N$ is the sea surface height. It must be determined to an accuracy of 2-3 cm.

The geoid:

Steady state sea level (in the absence of external forces, winds tides, eddies) produced by the uneven distribution of the Earth's mass. At scales of 10 to 10000 km lateral gravity forces determine the surface topography. Gravity missions GOCE and GRACE

12.2 Shape of the Earth

365

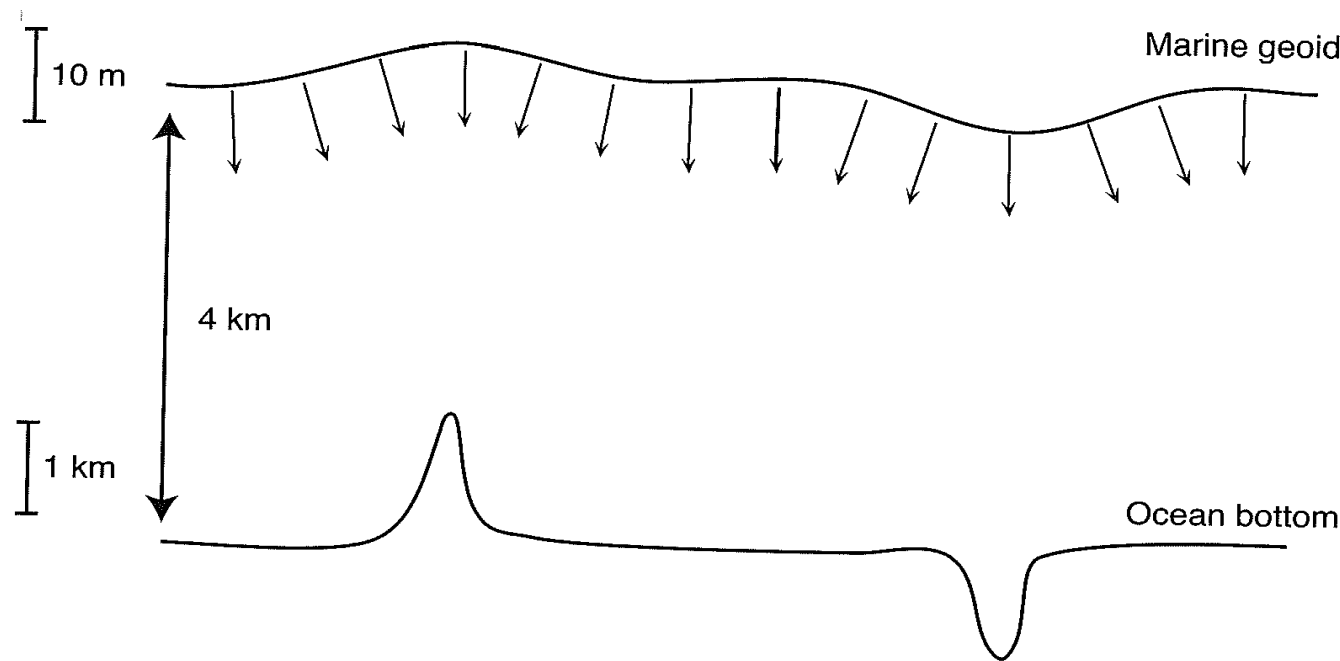


Fig. 12.2. The effect of a rise and depression in the seafloor topography on the marine geoid. The horizontal scale is of order 10 to 1000 km. The arrows show the local gravitational accelerations, which are normal to the geoid. (Adapted from Figure 10 of Chelton (1998) and from discussion in Smith (2010).)

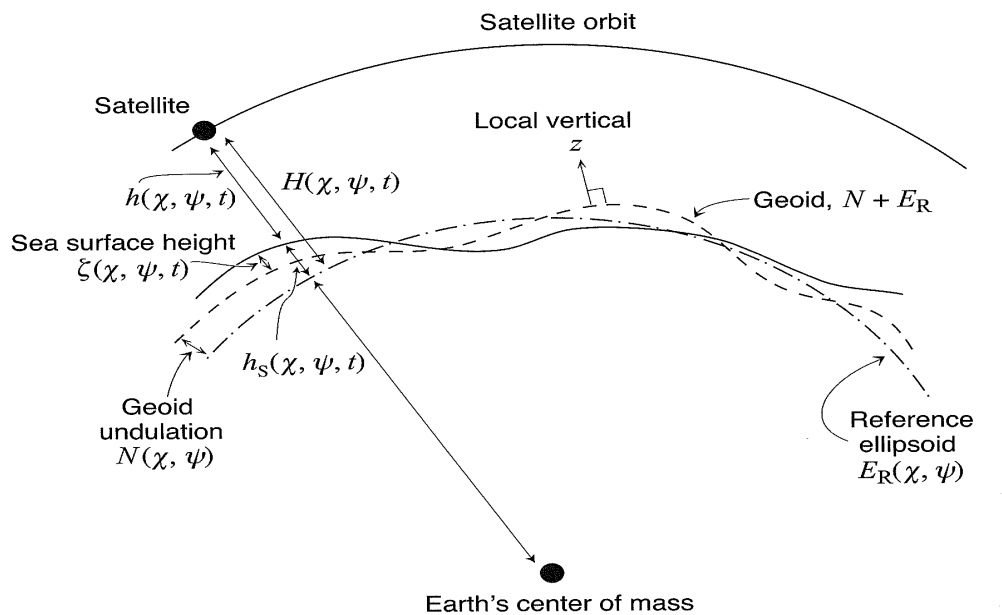
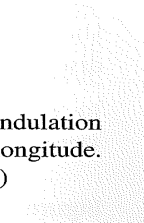


Fig. 12.1. The altimeter geometry showing the satellite orbit, the reference ellipsoid, geoid undulation and height of the sea surface above the Earth's center of mass, where χ is latitude and ψ is longitude. See the text for further description. (Adapted from Figure 3, Wunsch and Stammer (1998).)



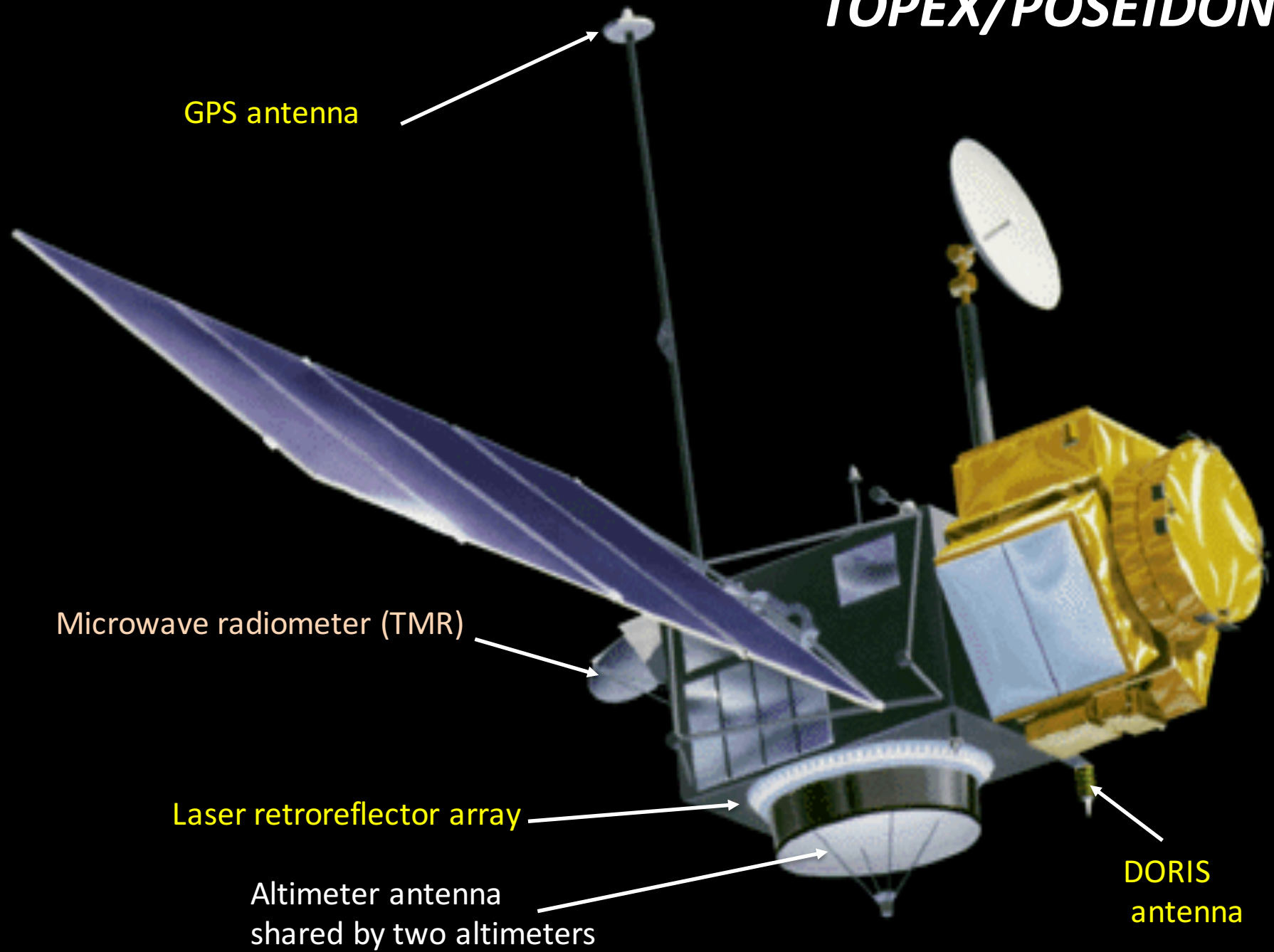
The altimeter measures the height h . h is affected by the ionospheric free electrons (**2 altimeters**), the water vapor and the cloud liquid water (**microwave radiometer**).

H is the height of the satellite above the ellipsoid. This requires to determine the precise position of the satellite (in 3D). Three methods: **GPS, DORIS, Laser retroreflector**

N is the geoid. This is the steady-state sea level (in the absence of external forces, winds tides, eddies) produced by the uneven distribution of the Earth's mass.

$\zeta = H - h - N$ is the sea surface height. It must be determined to an accuracy of 2-3 cm.

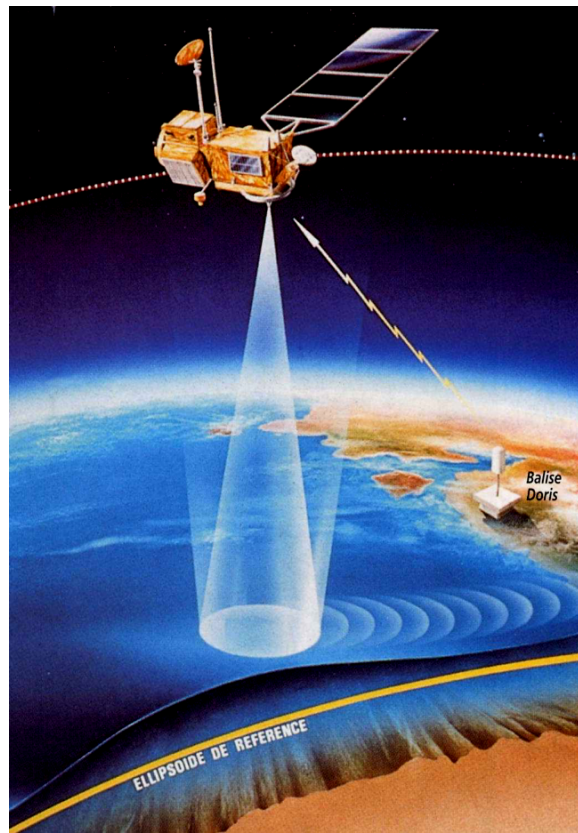
TOPEX/POSEIDON



Topex/Poseidon (1992-2006): a joint project between NASA and CNES

« The most successful ocean experiment of all time »

Walter Munk (Testimony Before the U.S. Commission on Ocean Policy, April 2002)



Temporal resolution: the time it takes for the satellite to repeat a particular orbit.

Spatial resolution: equatorial spacing between successive orbits.

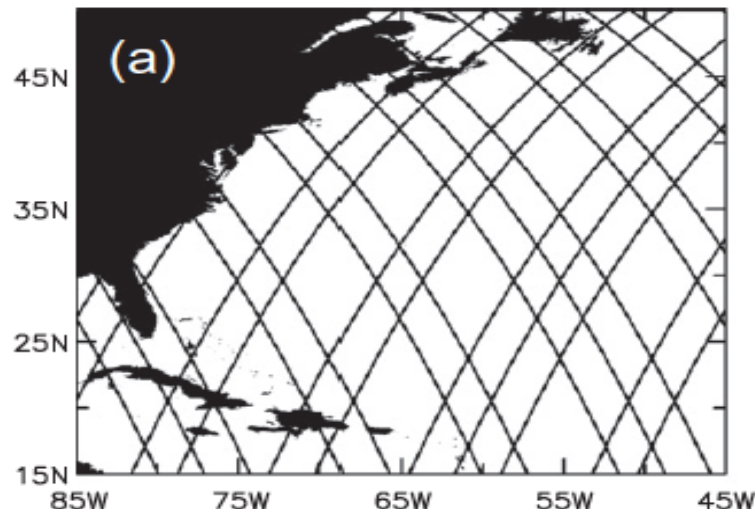
A short repeat period yields a large spatial separation: Topex/Poseidon
A long repeat period yields a small spatial separation: ERS-1

Topex/Poseidon (1992-2006): 10 days and 320 km (altitude of 1336 km)

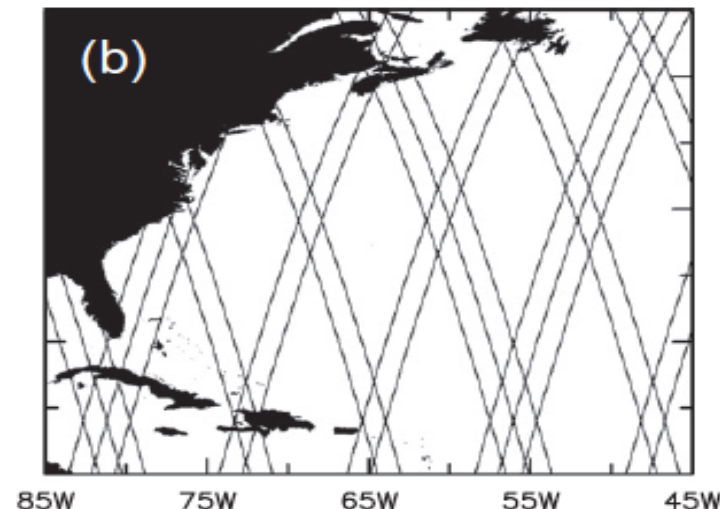
ERS-1 (1991-1996): 35 days and 90 km (altitude of 785 km)

Better to use several altimeters ...

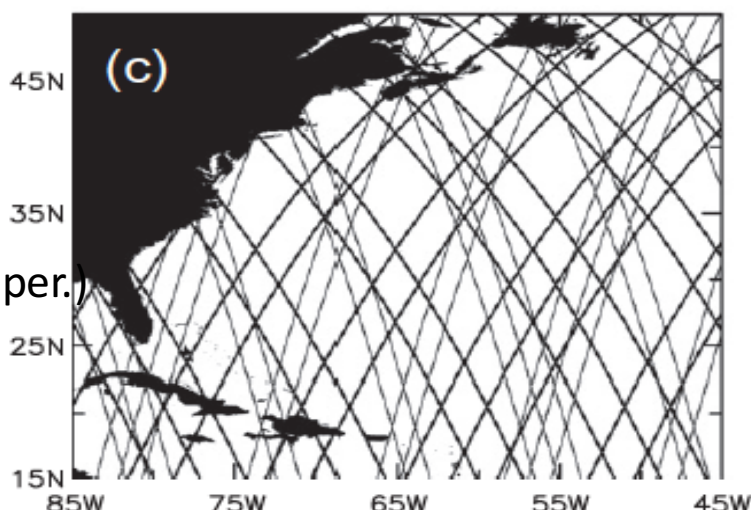
T/P (7 day period)



ERS-1 (7 day period)



T/P +
ERS-1
(7 day per.)



T/P +
ERS-1
(35 day per.)

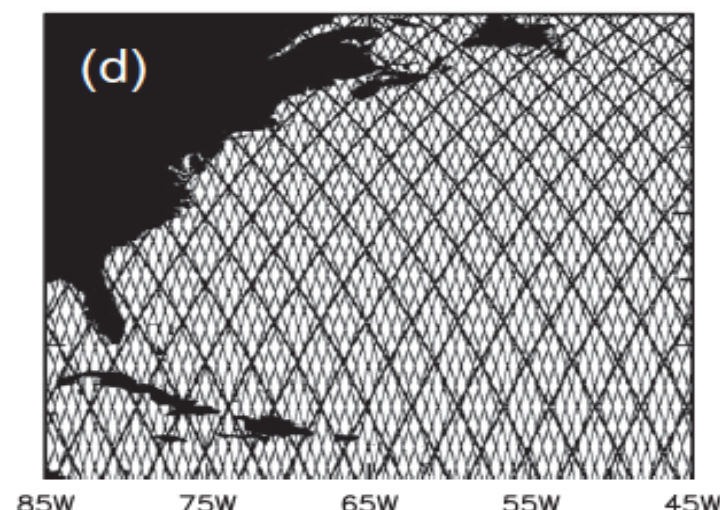
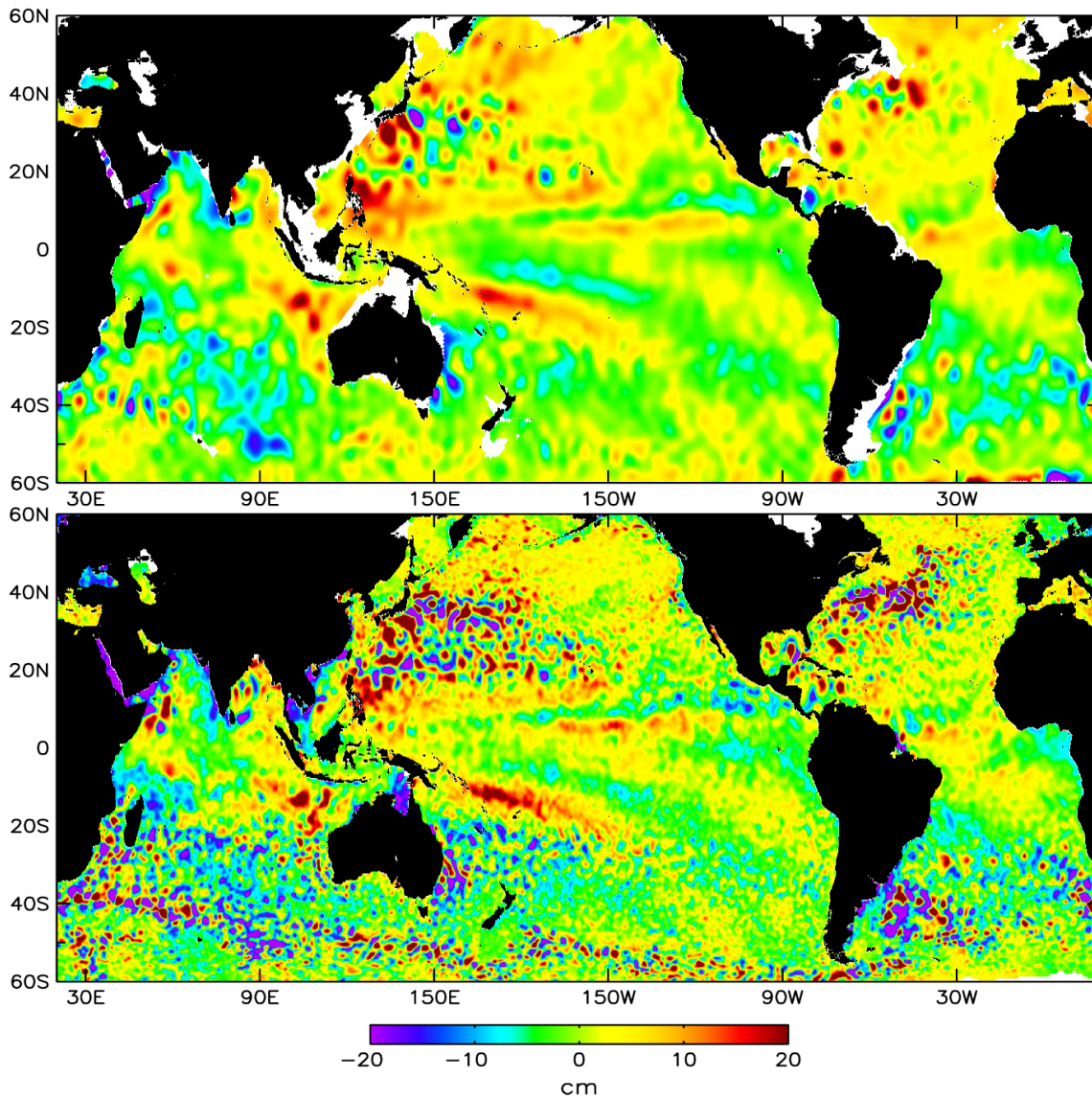
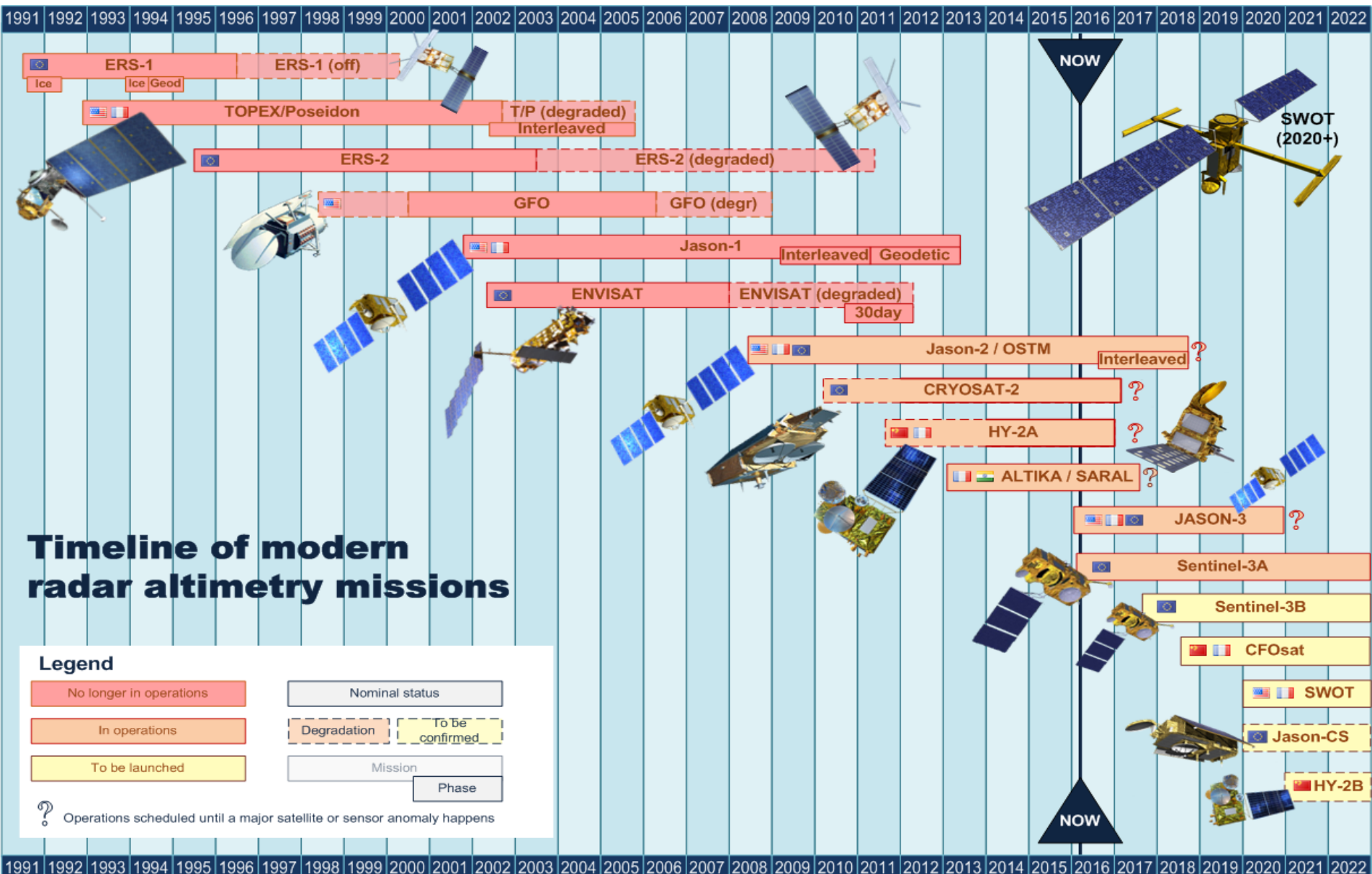


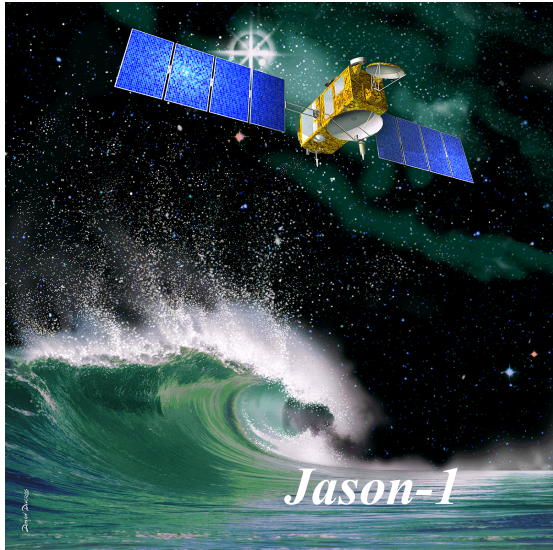
Fig. A4. The ground track patterns for the 10-day repeat orbit of T/P and its successors Jason-1 and Jason-2 (thick lines) and the 35-day repeat orbit of ERS-1 and its successors ERS-2 and Envisat (thin lines). (a) The ground tracks of the 10-day orbit during a representative 7-day period; (b) The ground tracks of the 35-day orbit during the same representative 7-day period; and (c) The combined ground tracks of the 10-day orbit and the 35-day orbit during the 7-day period; and (d) The combined ground tracks of the 10-day orbit and the 35-day orbit during the full 35 days of the 35-day orbit.

Better to use several altimeters ...



Satellite altimetry provides: global coverage, all weather, real-time SSH measurements





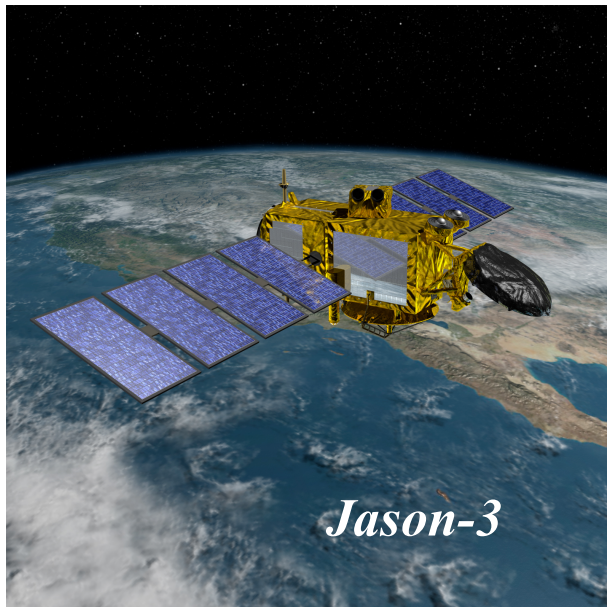
Jason-1

Launched in December 2001. Same design as TOPEX/POSEIDON. Its mass is only 500 kg (2400 kg for T/P).



Jason-2

Launched in June 2008.
Same design as JASON-1.



Jason-3

Launched in January 2016.
Same design as JASON-2

Satellite altimetry provides global coverage, all weather, real-time SSH measurements

Since SSH can be directly related to ocean circulation through the geostrophic approximation

⇒ Satellite altimetry allows to estimate the ocean circulation on a global scale and in real time.

Almost 25 years after, results obtained from satellite altimetry are outstanding

What are these results?

Two classes of results:

Results from along track analysis: spectral characteristics of the ocean variability.

Results from merged gridded products. Trackings of ocean eddies in the world's ocean

Along track analysis: SSH spectrum

A satellite radar altimeter provides a snapshot of an SSH profile along its ground tracks, revealing the spatial structure of ocean variability that is not available from in-situ observations.

The SSH spectrum, displays the distribution of SSH variance at different scales. It has been **the most popular topic of investigation since the early days of satellite altimetry**.

Referring to the **existing theories** of geostrophic turbulence the spectrum slope can be interpreted as an indicator of the dynamic processes governing this turbulence.

Thus Charney (1966, 1971) **theory of geostrophic turbulence predicted a k^{-3} spectrum slope** for the kinetic energy of the horizontal velocity components. Blumen (1978) predicted a **k^{-2} spectrum slope for surface geostrophic turbulence**.

If this is true for the ocean,

a k^{-3} spectrum for kinetic energy should lead to a k^{-5} spectrum for SSH!

a k^{-2} spectrum for kinetic energy should lead to a k^{-4} spectrum for SSH!

Fu L. L. JGR 1983: Mesoscale variability from SEASAT

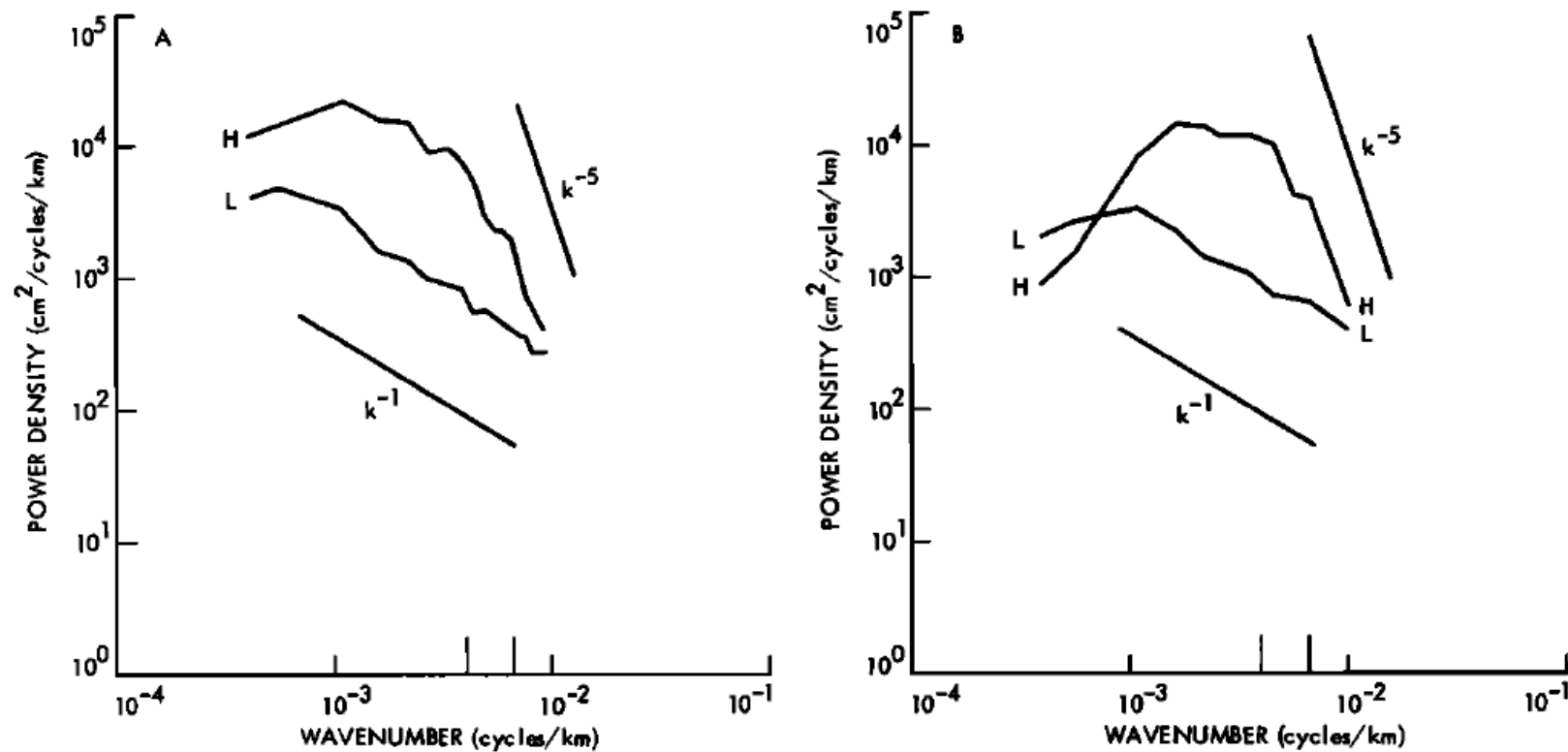
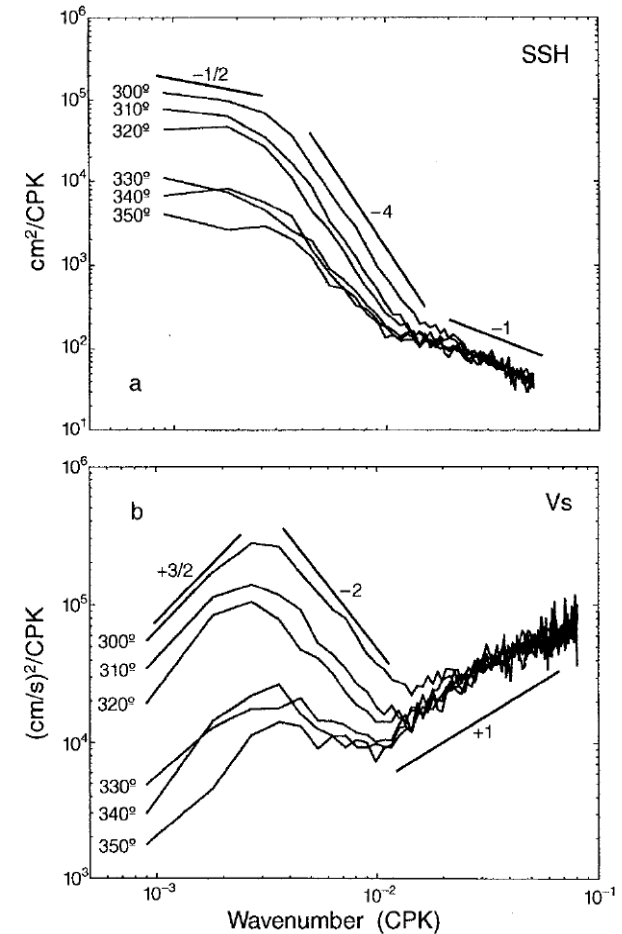


Fig. 7. (a) The average spectra of residual sea-surface height for the high-energy areas (labeled by H) and the low-energy areas (labeled by L). (b) The corresponding scalar-wave-number spectra. The two large tick marks on the wave number axis indicate wavelengths of 150 km and 250 km, respectively.

=> Close to geostrophic turbulence ...

Stammer, JPO 1997 : Global characteristics from Topex/Poseidon data: Extratropical wavenumber spectra suggest a geostrophically turbulent ocean. They are basically uniform in shape and show a plateau on long wavelength for SSH and a steep spectral decay close to k^{-5} toward smaller wavelengths.



Significant differences between the Western and Eastern parts of the oceanic basins ...

FIG. 13. TOPEX/POSEIDON mean alongtrack wavenumber spectra for (a) sea surface height and (b) cross-track velocity from various $10^\circ \times 10^\circ$ areas between 30° and 40°N with center longitudes indicated in the figure.

Le Traon et al., JPO 2008: T/P, Jason 1 Geosat follow on, Envisat

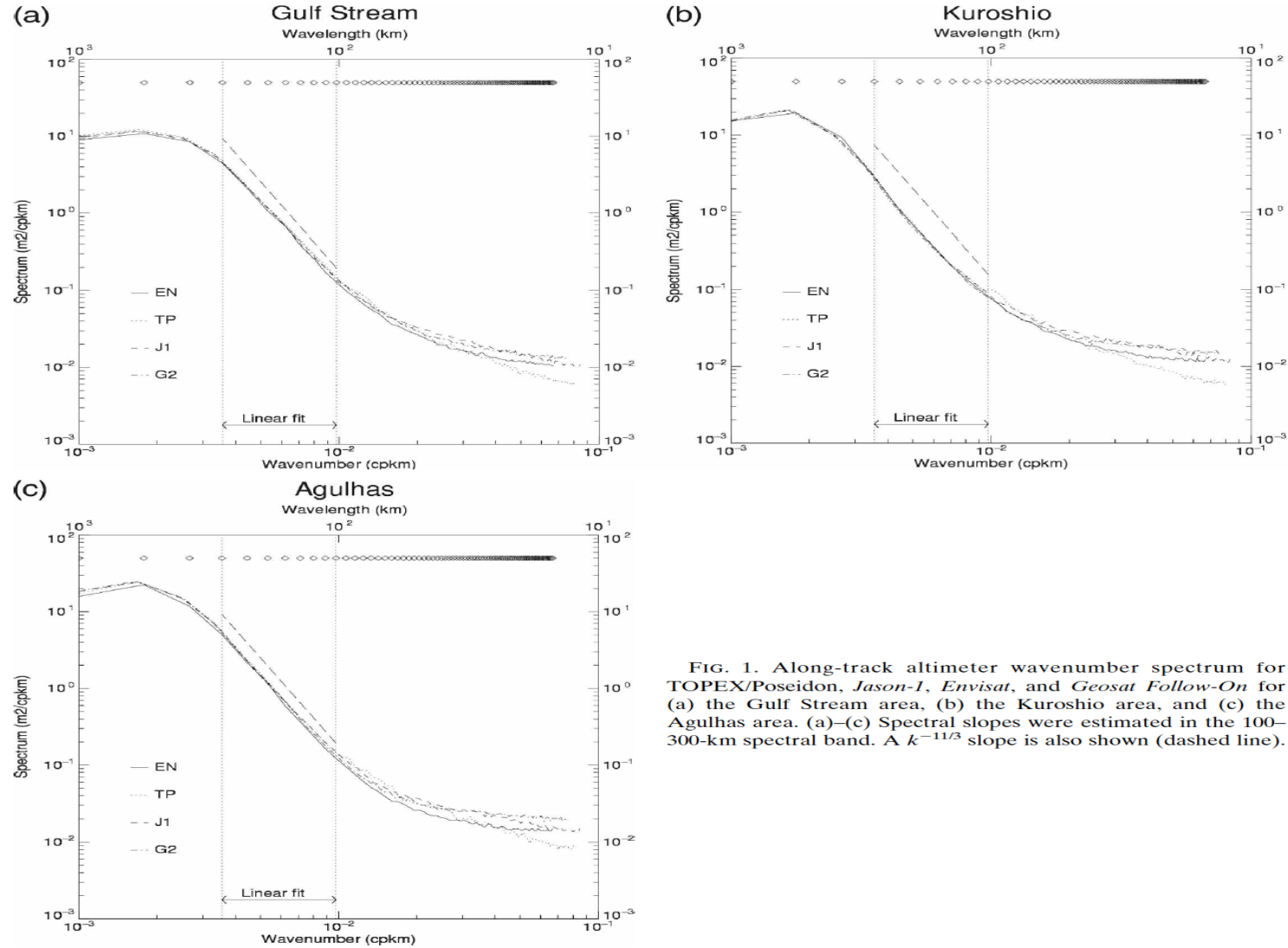


FIG. 1. Along-track altimeter wavenumber spectrum for TOPEX/Poseidon, Jason-1, Envisat, and Geosat Follow-On for (a) the Gulf Stream area, (b) the Kuroshio area, and (c) the Agulhas area. (a)–(c) Spectral slopes were estimated in the 100–300-km spectral band. A $k^{-11/3}$ slope is also shown (dashed line).

=> Close to surface quasigeostrophic turbulence ...

Y. Xu and L.L. Fu (JPO, 2012) using JASON-1 data:

- A key finding is that the spectral slopes are generally steeper than k^{-2} poleward of the 20 degree latitudes.
- Results indicate that the spectral slopes in the core **regions of the major ocean current** systems have values between the **original geostrophic turbulence theory** (k^{-5}) and the **surface quasigeostrophic theory** (k^{-4}).
- The near k^{-4} spectrum suggests that the sea surface height variability at these wavelengths in the high eddy energy regions might be governed by frontogenesis.

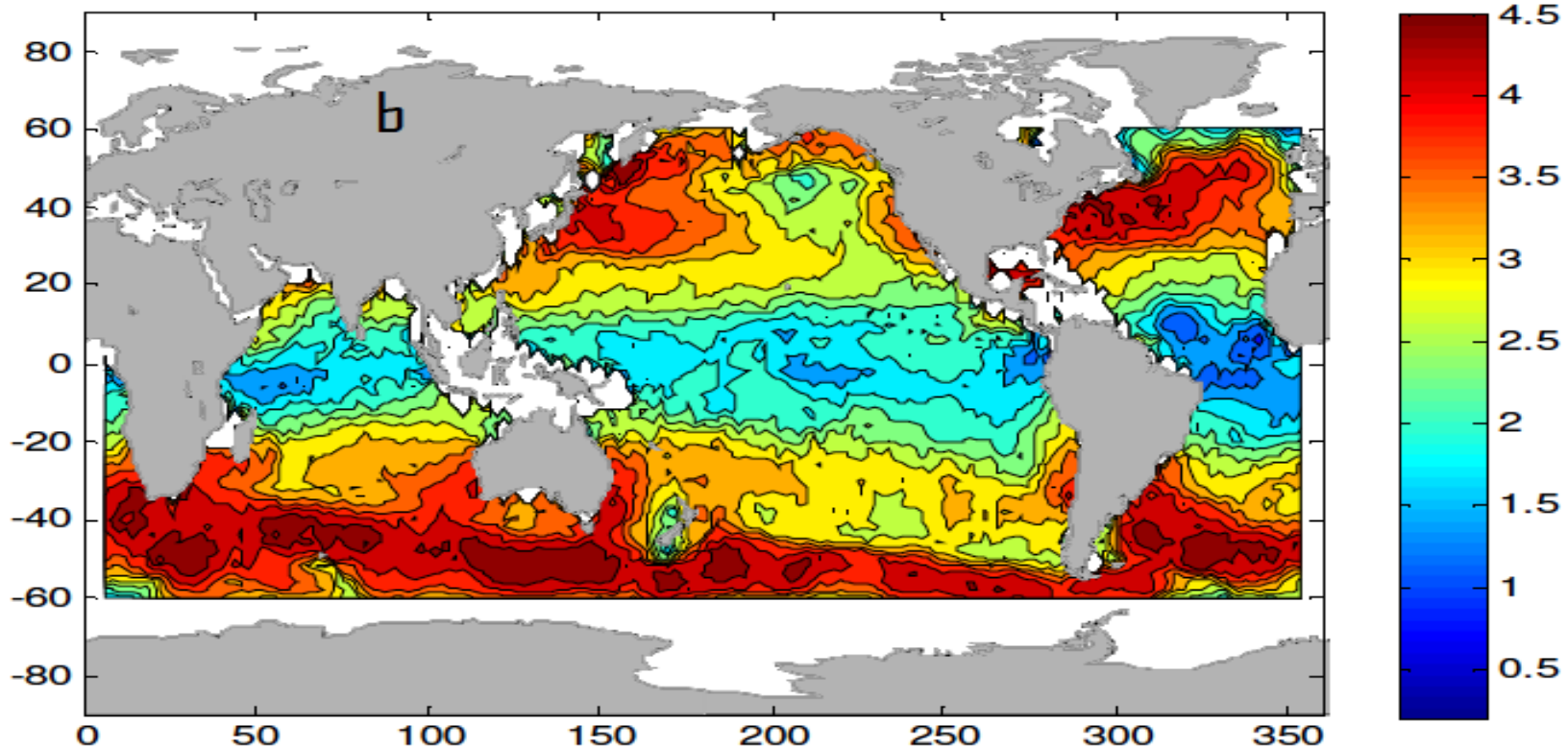
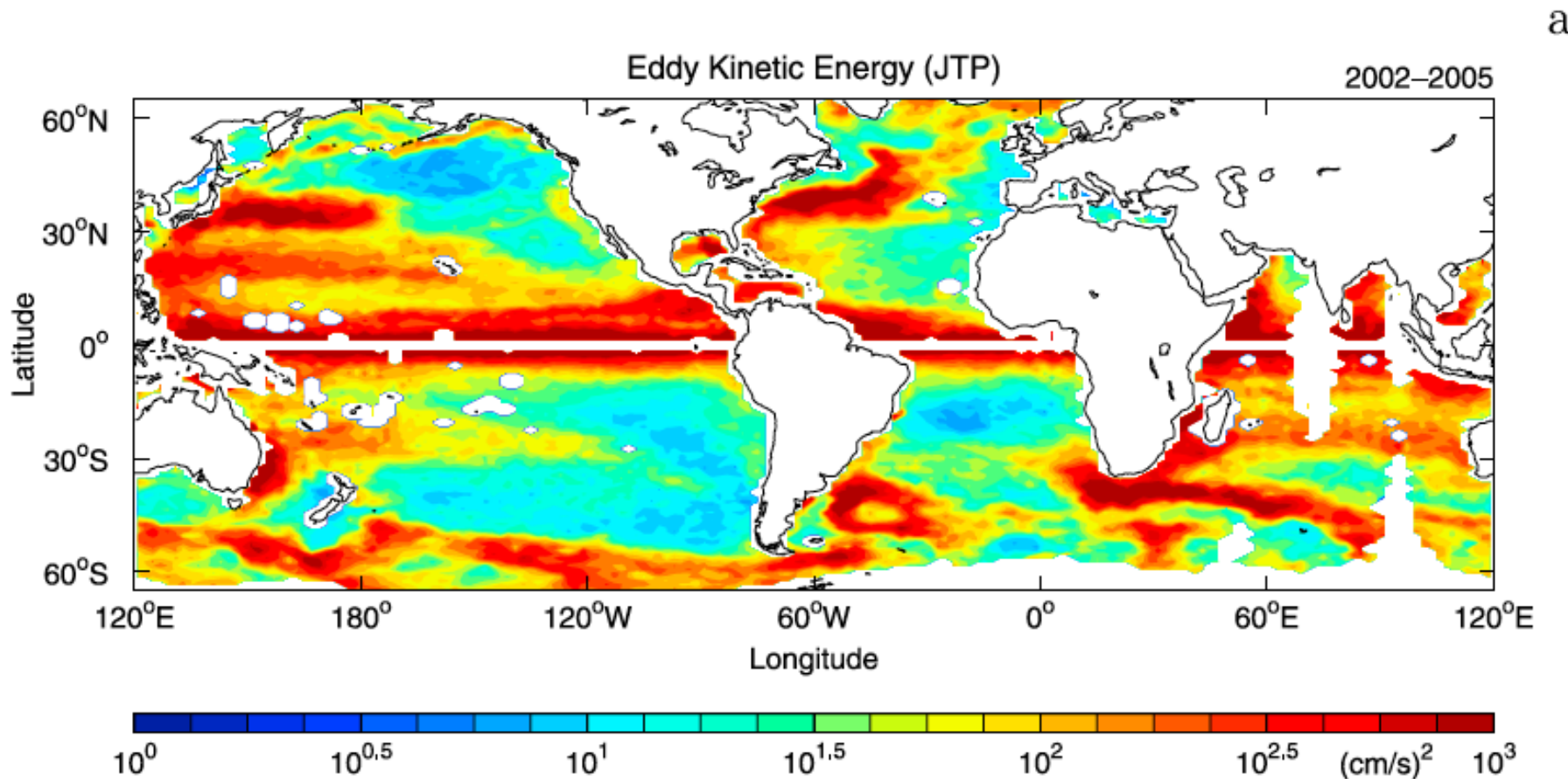


Fig. 3. The global distribution of the spectral slopes of SSH wavenumber spectrum in the wavelength band of 70–250 km estimated from the Jason-1 altimeter

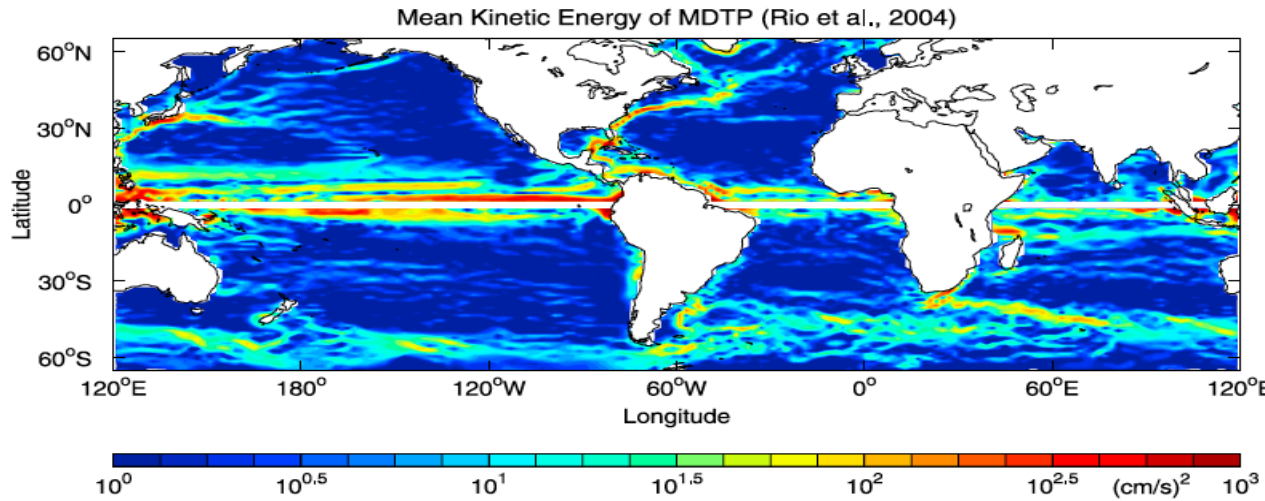
These results do not indicate the existence of a universal wavenumber spectrum and therefore of a universal dynamical regime in the world ocean

Scharffenberg & Stammer JGR 2010: Using T/P & Jason 1 mission data



Scharffenberg & Stammer JGR 2010: Using T/P & Jason 1 mission data

a



b

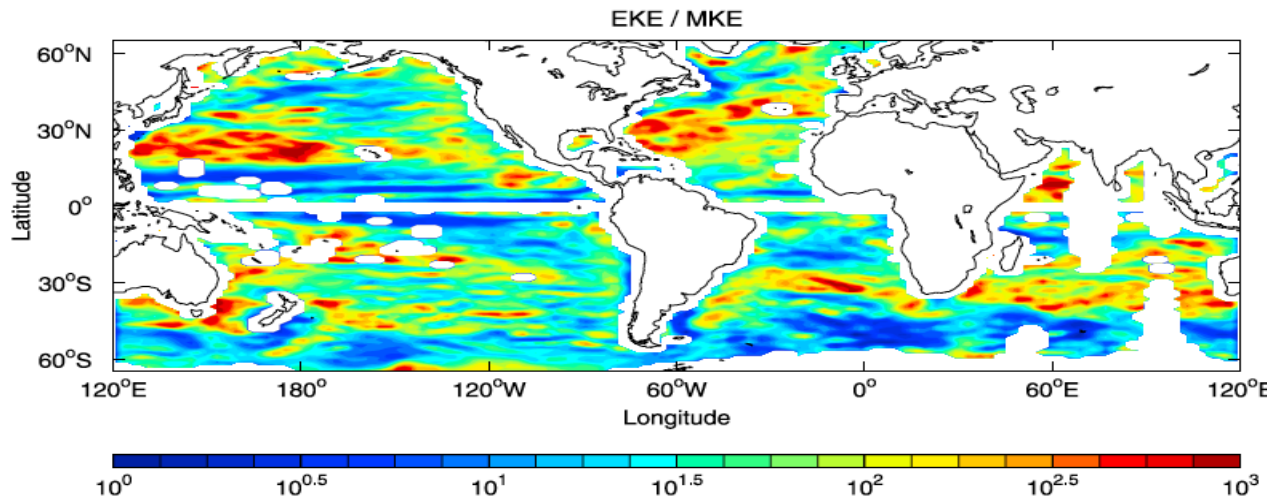
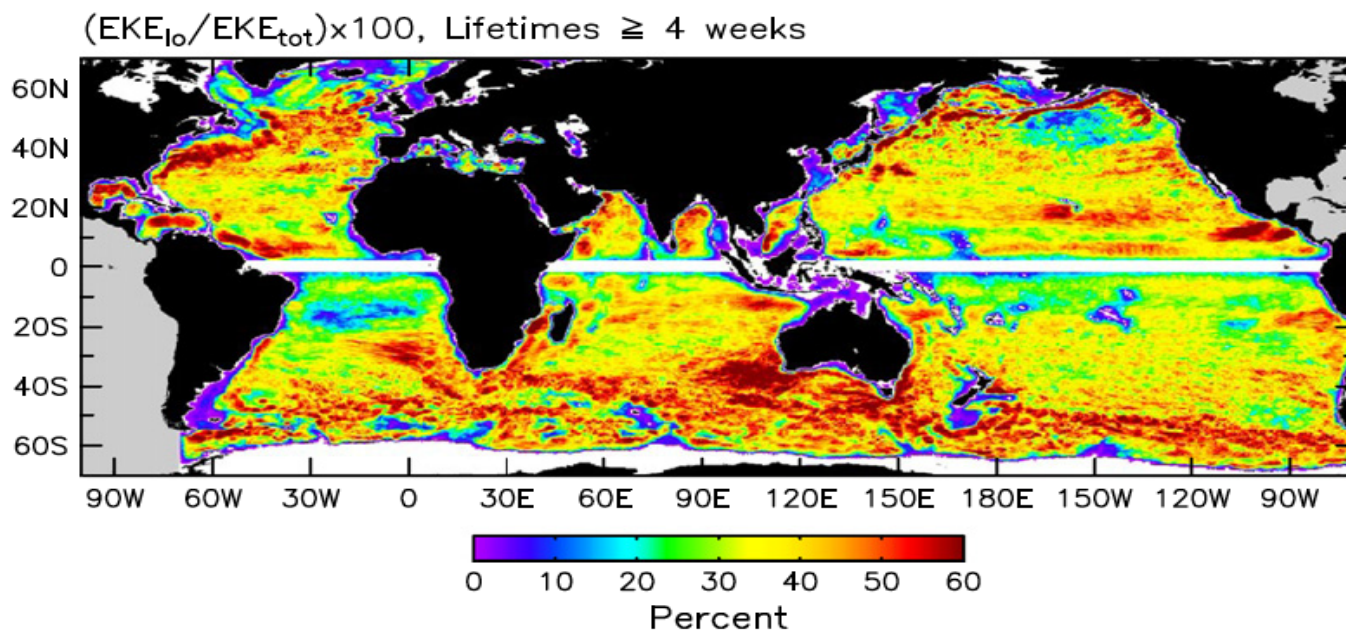
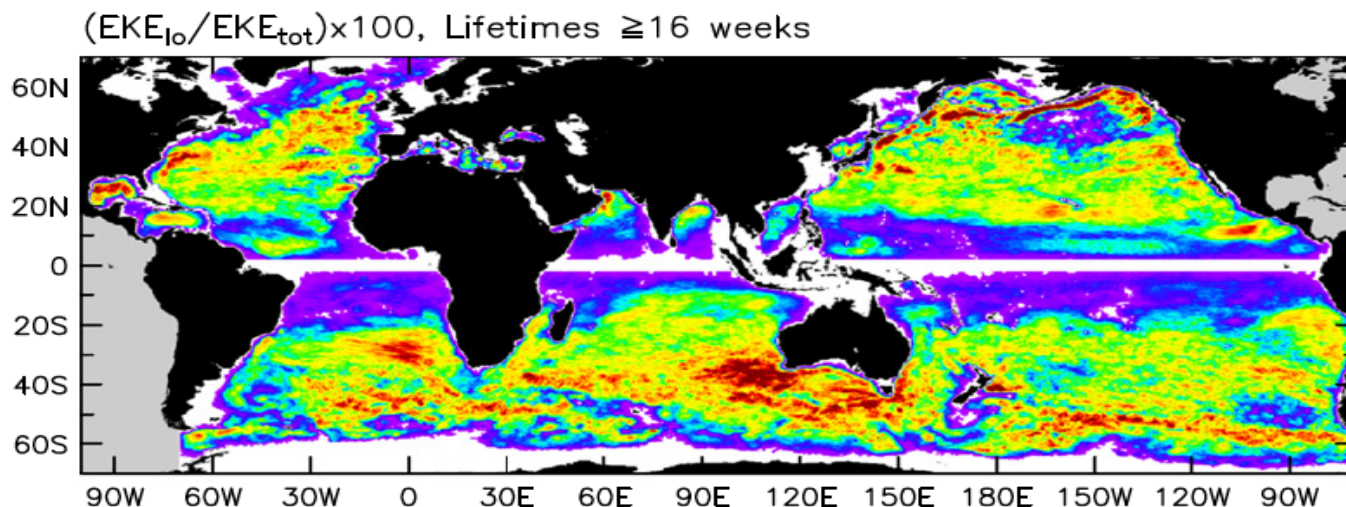


Figure 7. (a) MKE computed from the *Rio and Hernandez [2004]* MDTP for each $2^\circ \times 1^\circ$ grid cell. (b) Ratio of EKE from JTP (Figure 5a) and MKE, filtered with a $6^\circ \times 4^\circ$ running mean.

EKE > MKE*10 ! (only large eddies are resolved)

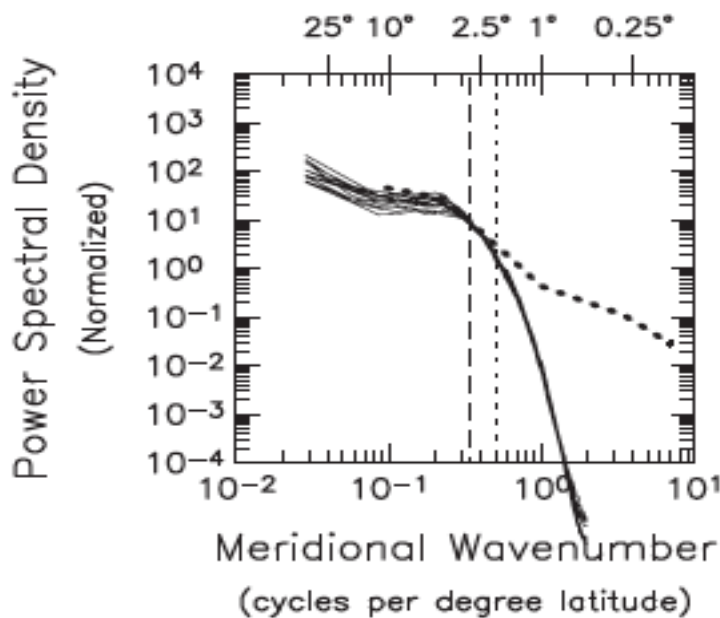
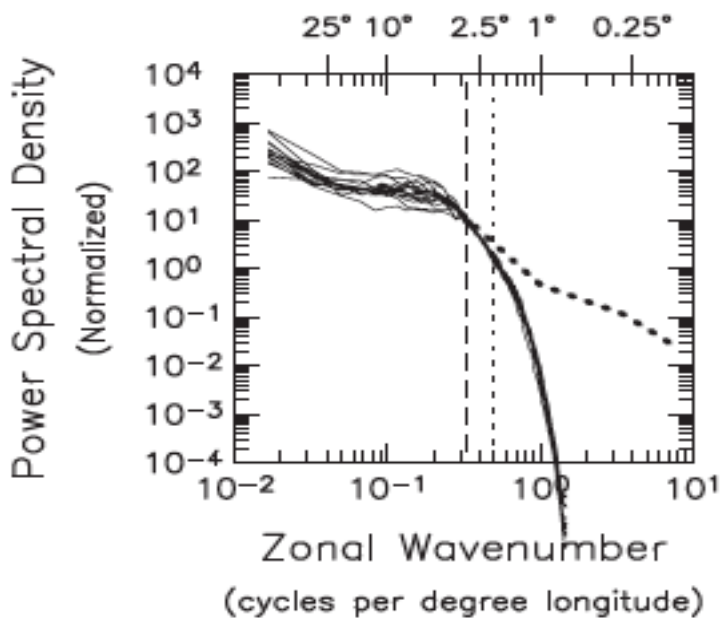
Similar result using 16 years of satellite altimetry (from Chelton et al., 2011)



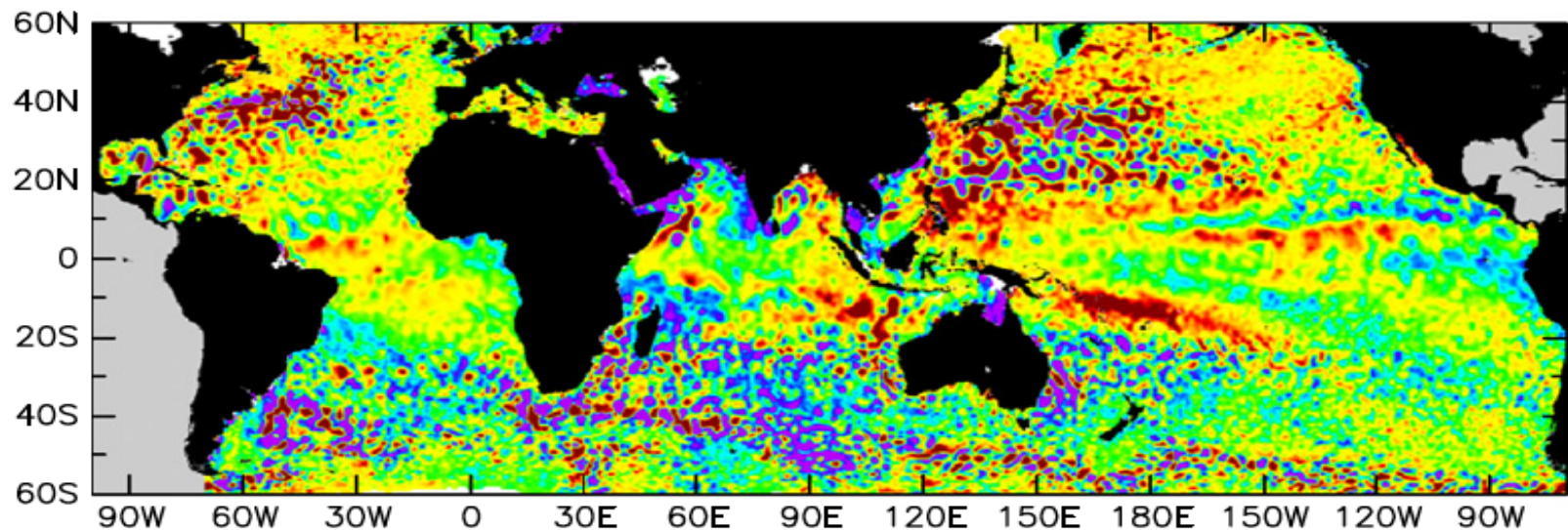
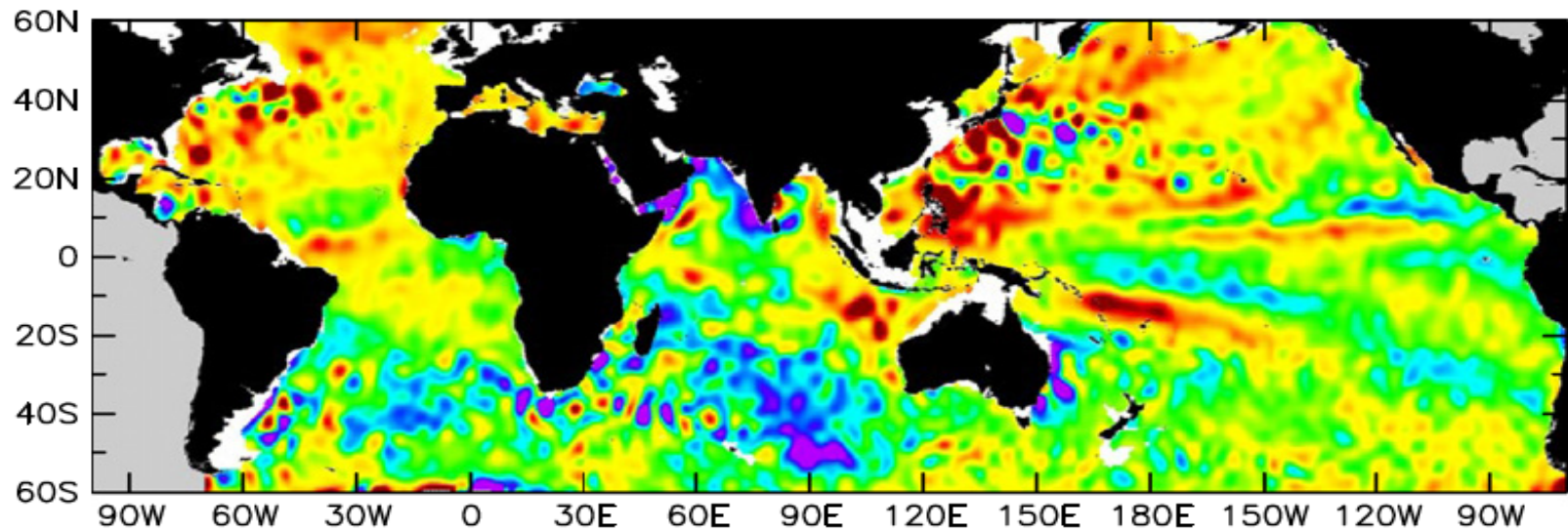
Results from merged gridded products.

AVISO products: gridded product is based on an objective analysis that assumes a Gaussian shape for eddies and low-pass filters along-track SSH anomalies to reduce measurement errors. The Mercator grid has $1/3^\circ$ ($1/4^\circ$) spacing. The dataset covers the period from Oct. 1992 up to now!

⇒ Only large scale eddies are retained



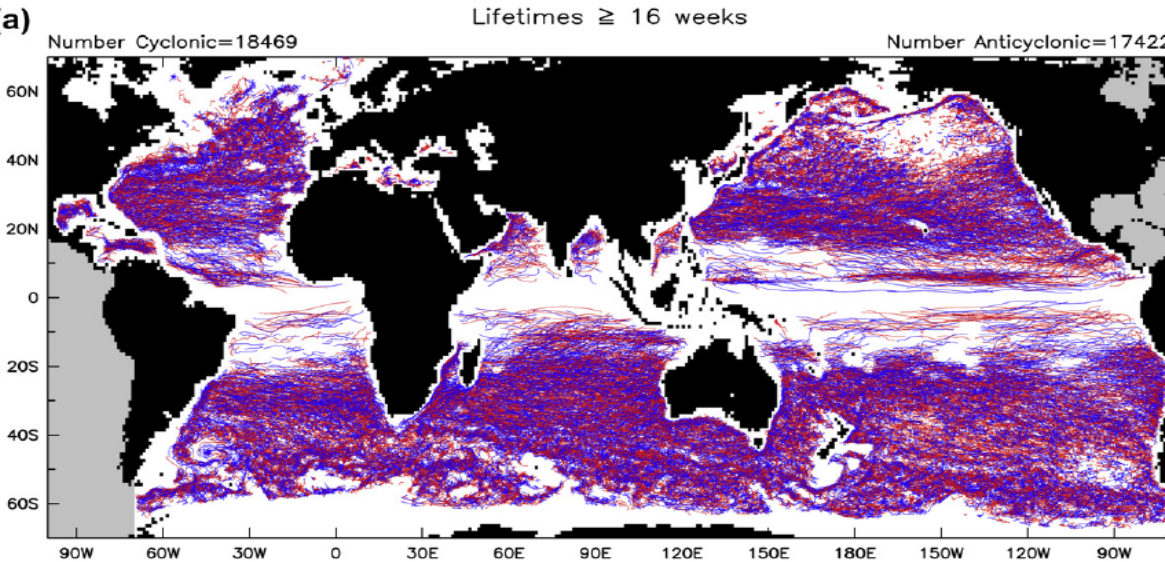
⇒ AVISO merged data revealed the prevalence of mesoscale eddies throughout most of the world's ocean



Global maps of SSH on August 1996 constructed from Topex/Poseidon (T/P) data only (top) and from the merged T/P and ERS-1 data in the AVISO reference series (bottom).
(From Chelton et al., P.O. 2011)

Tracking of eddies around the world's ocean using OW parameter (Chelton et al. PO 2011)

(a)



(b)

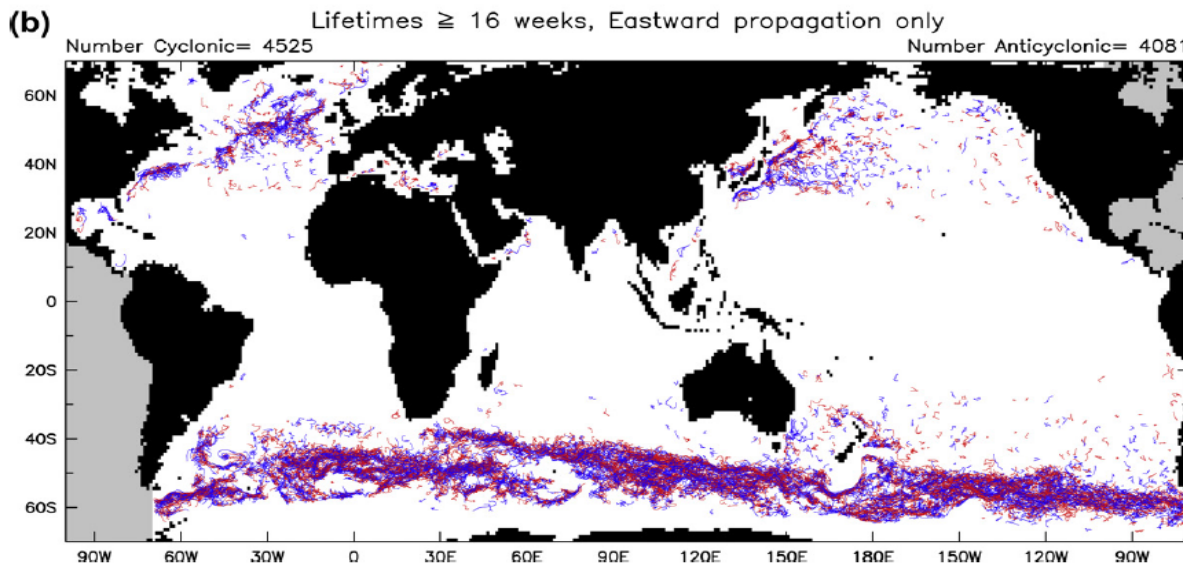


fig. 4a and b. The trajectories of cyclonic (blue lines) and anticyclonic (red lines) eddies over the 16-year period October 1992–December 2008 for (a) lifetimes \geq 16 weeks and (b) lifetimes \geq 16 weeks for only those eddies for which the net displacement was eastward. The numbers of eddies of each polarity are labeled at the top of each panel.

Nonlinearities of the eddies (Chelton et al. PO 2011)

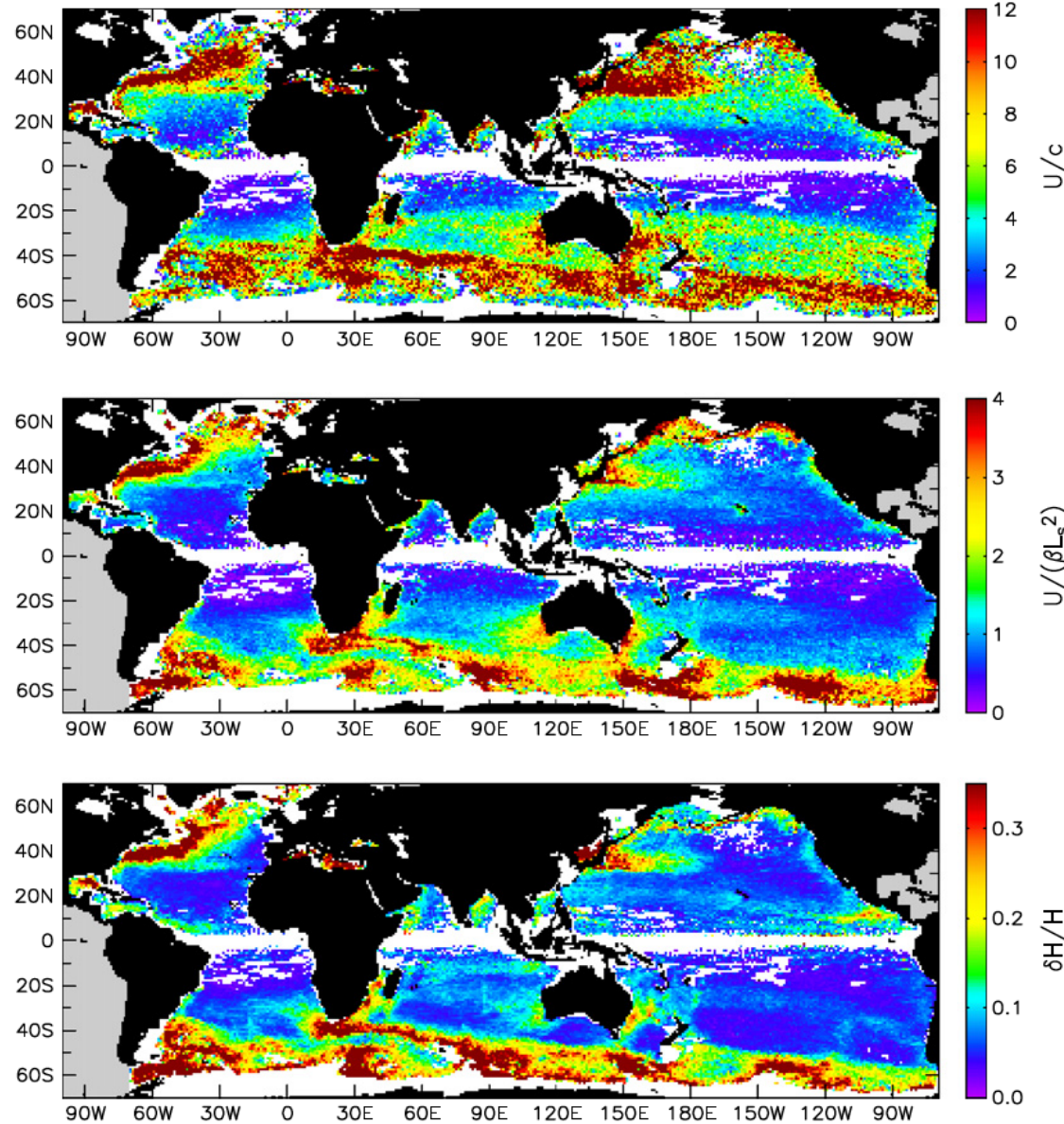


Fig. 17. Maps of the average values of the three nonlinearity parameters in Fig. 16 for each $1^\circ \times 1^\circ$ region. Top to bottom: the advective nonlinearity parameter U/c ; the quasi-geostrophic nonlinearity parameter $U/(\beta L_s^2)$; and the upper-layer thickness nonlinearity parameter $\delta H/H$.

Propagation characteristics

Eddies propagating westward over distance $> 10^\circ$ of longitude

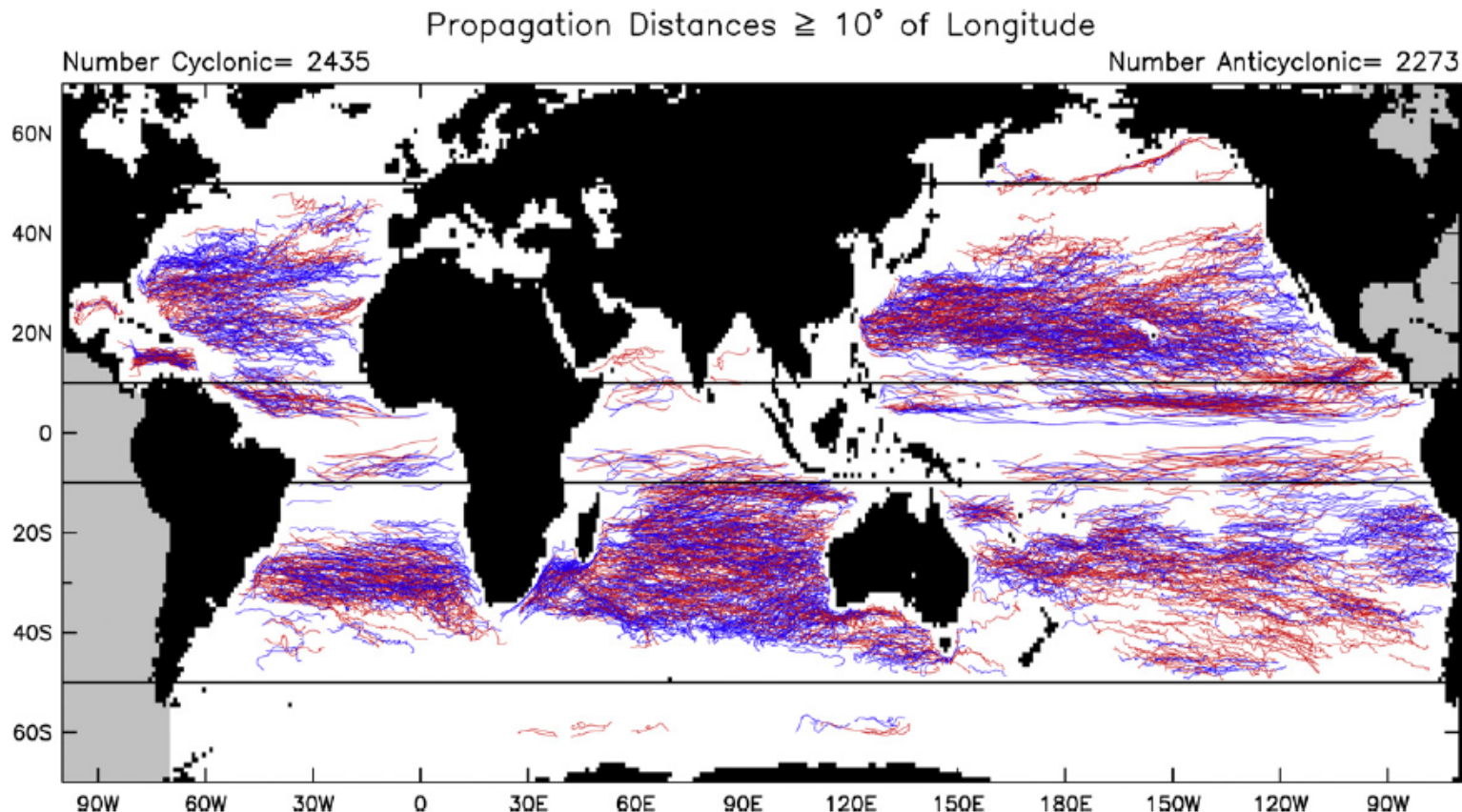


Fig. 18. The trajectories of all of the 2435 cyclonic (blue lines) and 2273 anticyclonic (red lines) eddies over the 16-year period October 1992–December 2008 that had lifetimes ≥ 16 weeks and propagated westward a minimum of 10° of longitude. The horizontal lines show the latitude ranges of $10\text{--}50^\circ$ that were considered for the analyses in Figs. 19 and 20.

(from Chelton et al., 2011)

Propagation characteristics

Eddies propagating westward over distance $> 10^\circ$ of longitude (from Chelton et al., 2011)

=>**Poleward drift for cyclonic eddies and equatorward for anticyclonic ones!**

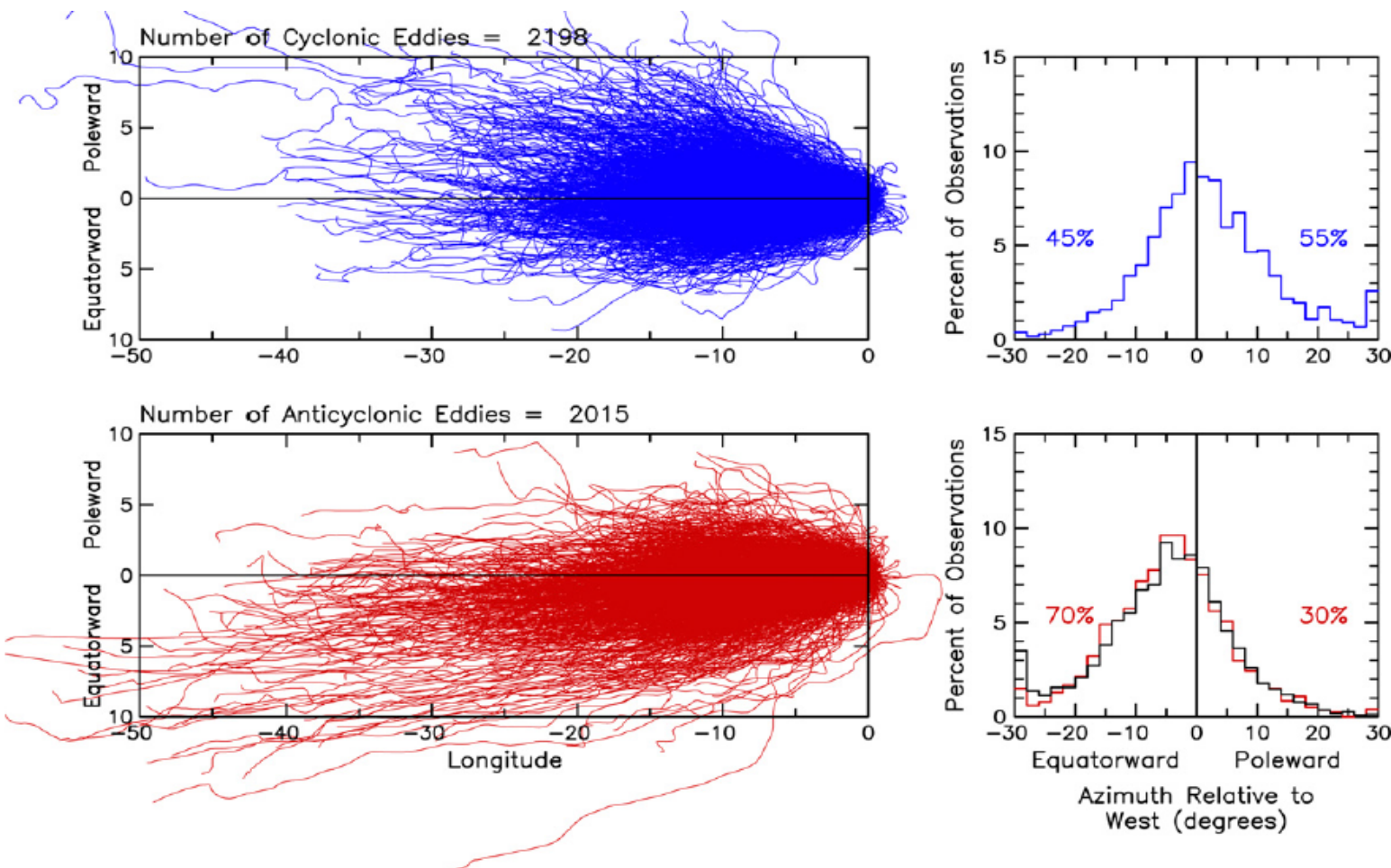


Fig. 20. The meridional deflections of the cyclonic (upper panels) and anticyclonic (lower panels) eddies with lifetimes ≥ 16 weeks and starting points at latitudes between 10° and 50° of both hemispheres that propagated westward a minimum of 10° of longitude (see Fig. 18). The left panels show the changes in longitude (negative westward) and latitude (positive for poleward and negative for equatorward of due west) relative to the initial location of each eddy. The right panels show histograms of the average azimuth of each eddy trajectory, defined as in Fig. 19. The labels in the right panels indicate the percentages of negative (left) and positive (right) eddy azimuths. The black line overlaid in the lower right panel corresponds to the histogram computed from the azimuths of the cyclonic eddies in the upper left panel that have been reflected about 0° and then shifted to have a median equal to the 4.3° equatorward median of the anticyclonic eddies.

Understanding the meridional drift on nonlinear eddies:
Hurricane example [see L. Shapiro (JAS, 1990, 1992)]

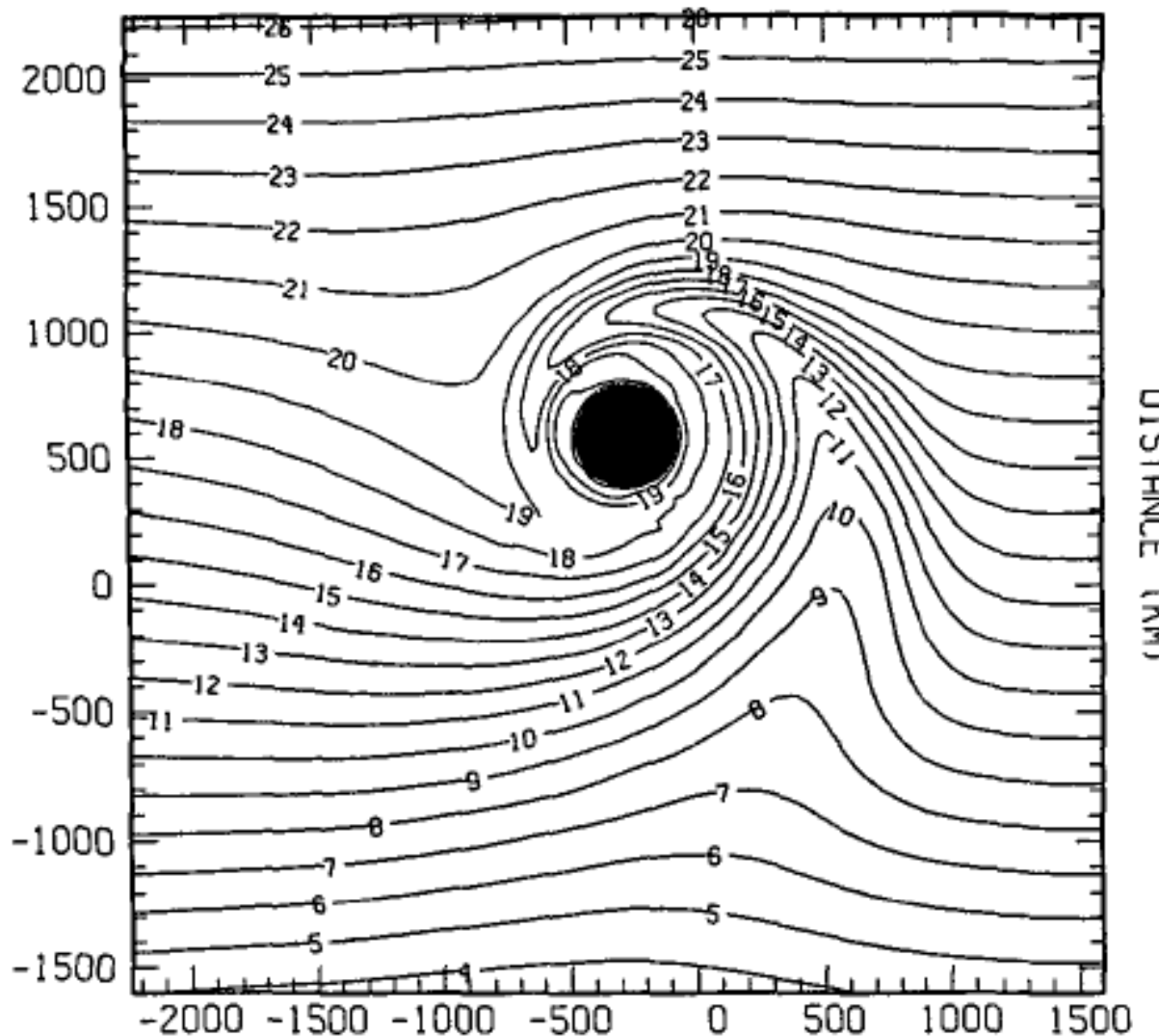


FIG. 6. Potential vorticity in the middle layer for a vortex on a β plane at 120 h. Contour interval is $1 \times 10^{-9} \text{ m}^{-1} \text{ s}^{-1}$.

Understanding the meridional drift on nonlinear eddies:
Hurricane example [see L. Shapiro (JAS, 1990, 1992)]

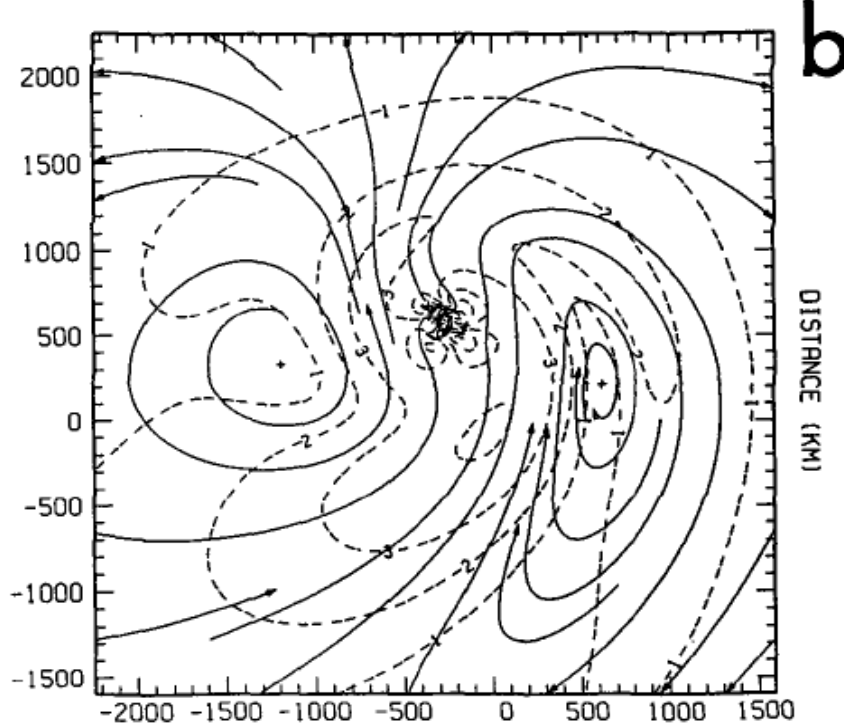
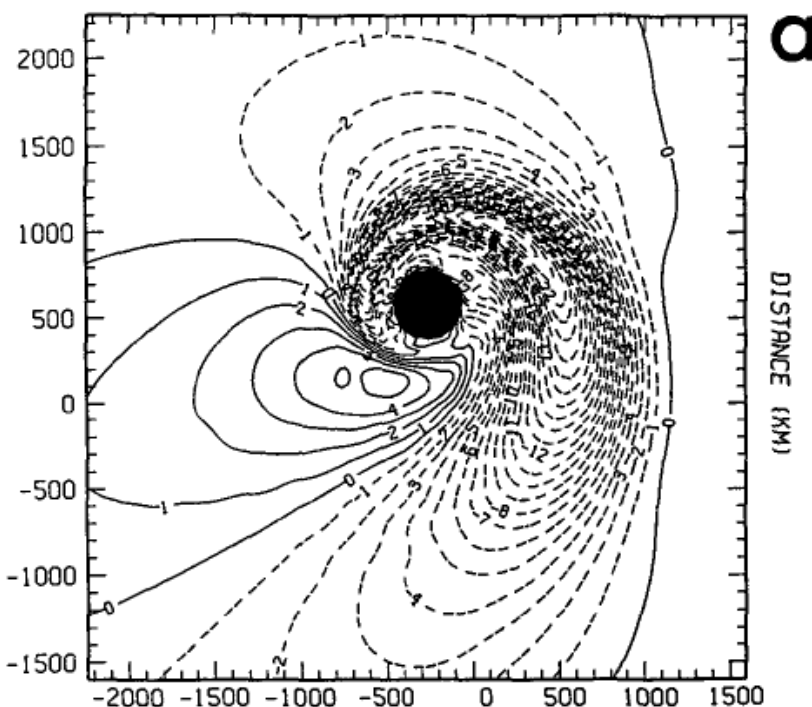


FIG. 7. (a) Relative vorticity (contour interval $1 \times 10^{-6} \text{ s}^{-1}$) and
(b) asymmetric wind (isotach interval 1 m s^{-1}) in the middle layer
for a vortex on a β plane at 120 h.

Understanding the meridional drift on nonlinear eddies:
Hurricane example [see L. Shapiro (JAS, 1990, 1992)]

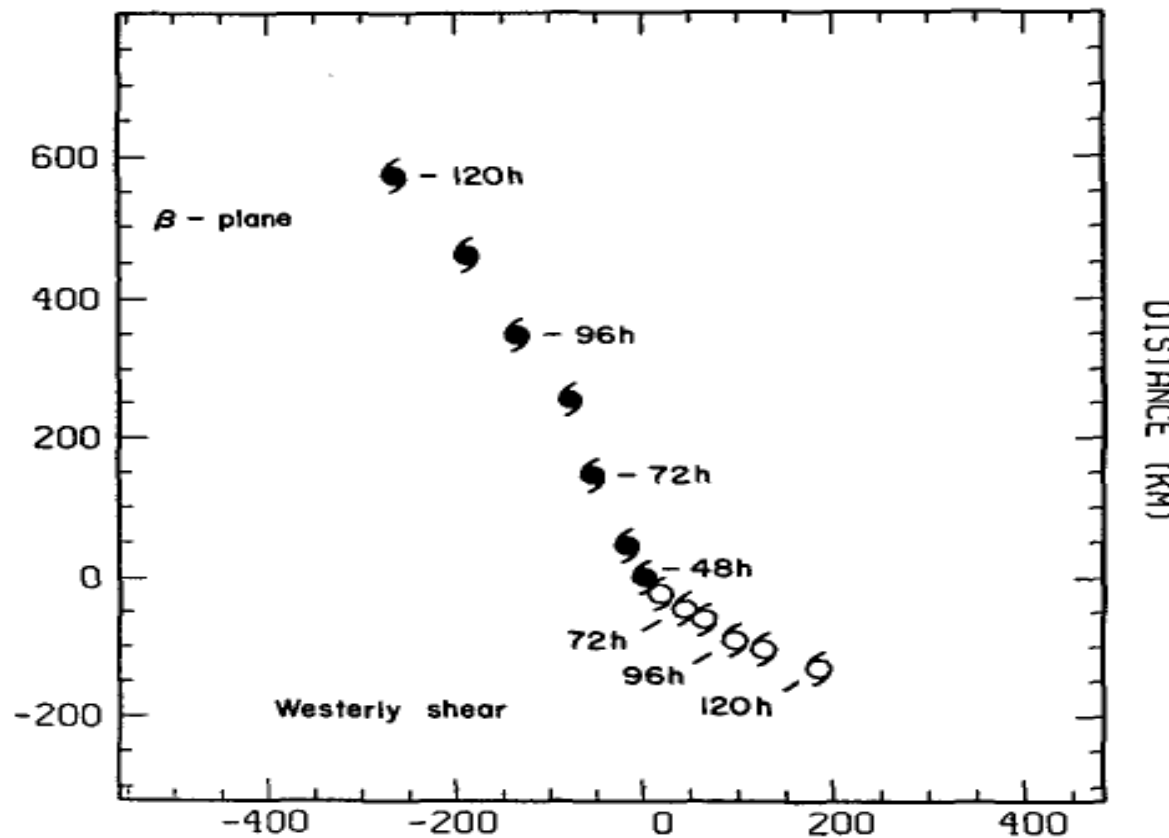


FIG. 4. Positions of vortex center, defined by minimum geopotential in middle layer, at 12-h intervals. Vortex on a β plane (solid symbols) moves to the northwest; vortex in westerly vertical shear (open symbols) moves to the southeast. Both simulations use symmetric vortex at 48 h as initial condition.

Eddy heat and salt transports:

One motivation to estimate eddy propagation characteristics from satellite altimetry is that, unlike Rossby waves, **eddies transport heat, salt and tracers in their core waters.**

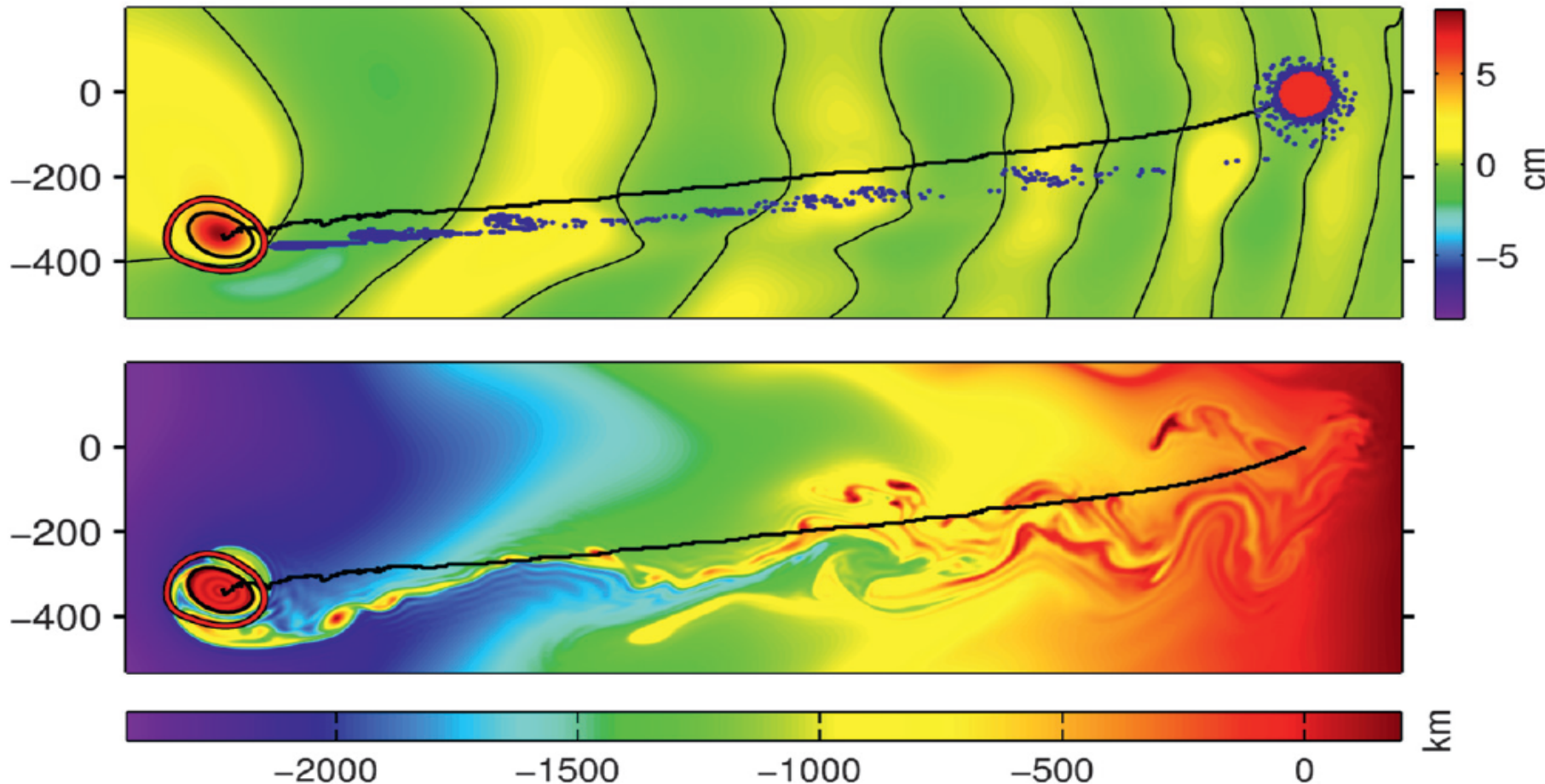


FIG. 13. Location of fluid advected on day 675. (top) SSH with the instantaneous trapped fluid contour (red) and relative vorticity zero contour (black). Blue circles show the day zero location of the floats in the eddy ring, whereas red circles show the location of floats in the eddy core. (bottom) A passive tracer equal to the initial (day 0) value of the zonal coordinate.

From Early et al., JPO 2011

First attempt from Dong et al. NC 2014: Satellite altimeter SSH data are used to track individual eddies and vertical profiles from co-located Argo floats are used to calculate T/S anomalies
=> Estimated meridional heat transport by eddies is similar to estimates from models
⇒ **Significant uncertainties primarily due to the paucity of the observational data, in particular in the ocean interior!!!.**

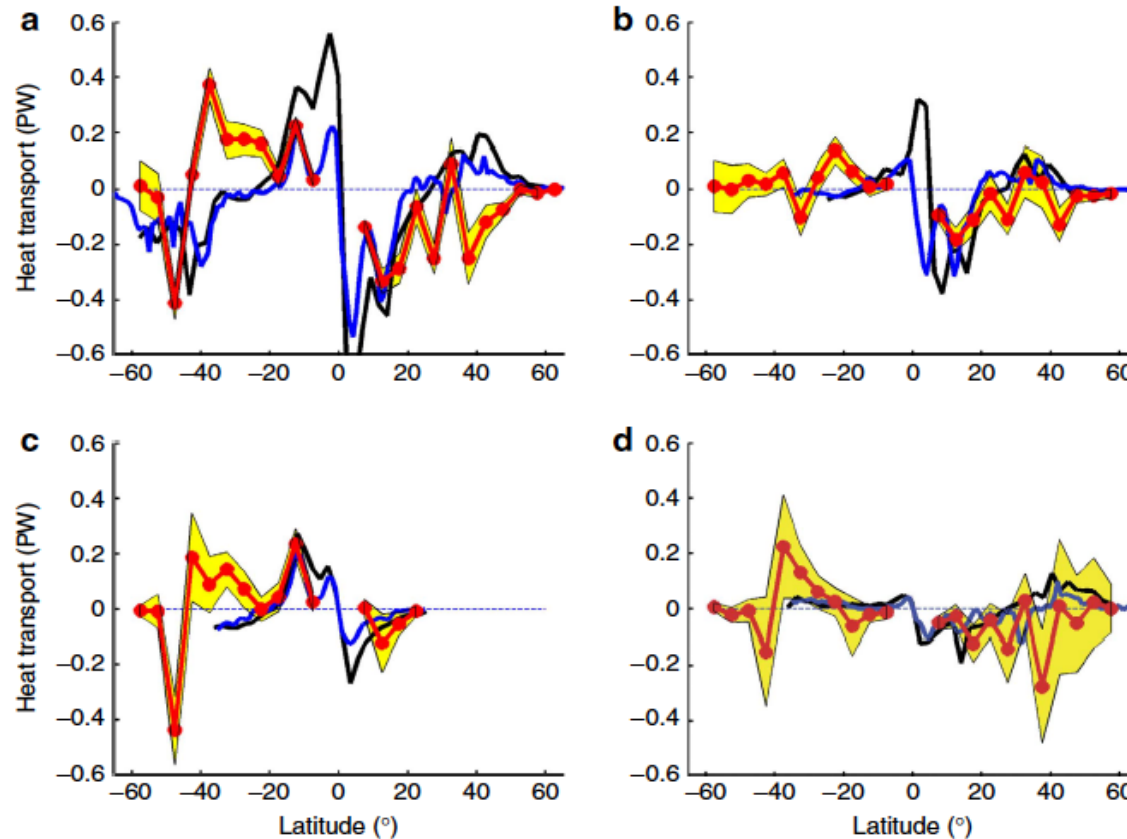


Figure 4 | Comparison with model results for eddy-induced heat transport. Comparison of zonally integrated, time-averaged meridional heat transports by eddy movement Q_h [PW] in red with Jayne and Marotzke¹ in black, and Volkov et al.², in blue: World Ocean (a), Pacific Ocean (b), Indian Ocean (c) and Atlantic Ocean (d). The uncertainty range of the eddy heat transport by the eddy movement is indicated by the yellow shading. The data from Jayne and Marotzke¹ are digitized from their paper, and Volkov et al.² provided their data to the authors.

Zhai et al. GRL 2008: AVISO Jan. 1995 – Dec. 2006:
Strong seasonality not well understood ...

L24609

ZHAI ET AL.: SEASONAL CYCLE OF EDDY KINETIC ENERGY

L24609

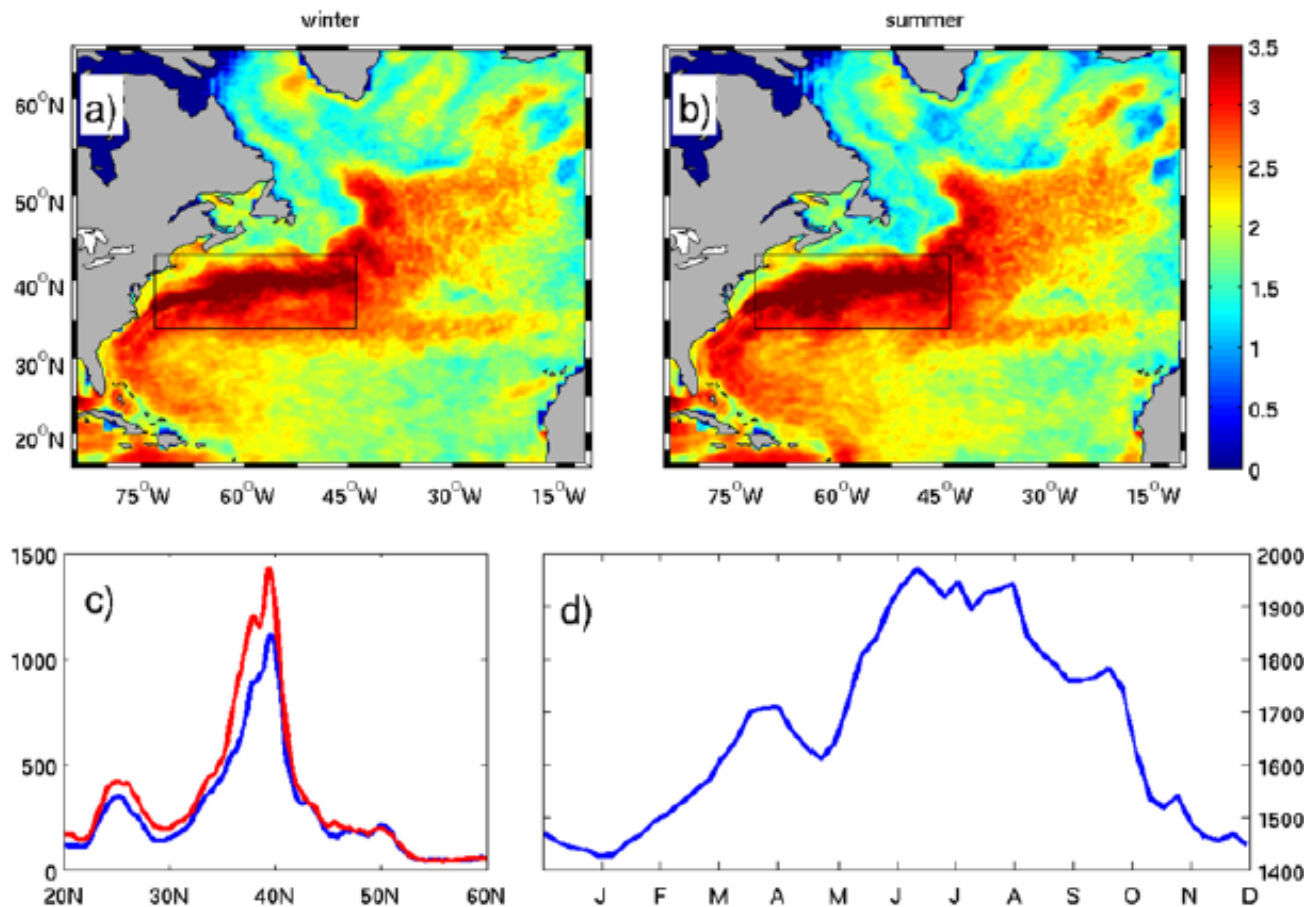


Figure 1. *EKE* averaged over (a) December, January and February and (b) June, July and August plotted on a log scale with base 10. (c) Cross-basin average of *EKE* from (Figure 1a; blue) and (Figure 1b; red) as a function of latitude and (d) seasonal cycle of *EKE* averaged in the rectangular box. Units: $\text{cm}^2 \text{ s}^{-2}$.

Zhai et al. GRL 2008: AVISO Jan. 1995 – Dec. 2006:
Strong seasonality not well understood ...

L24609

ZHAI ET AL.: SEASONAL CYCLE OF EDDY KINETIC ENERGY

L24609

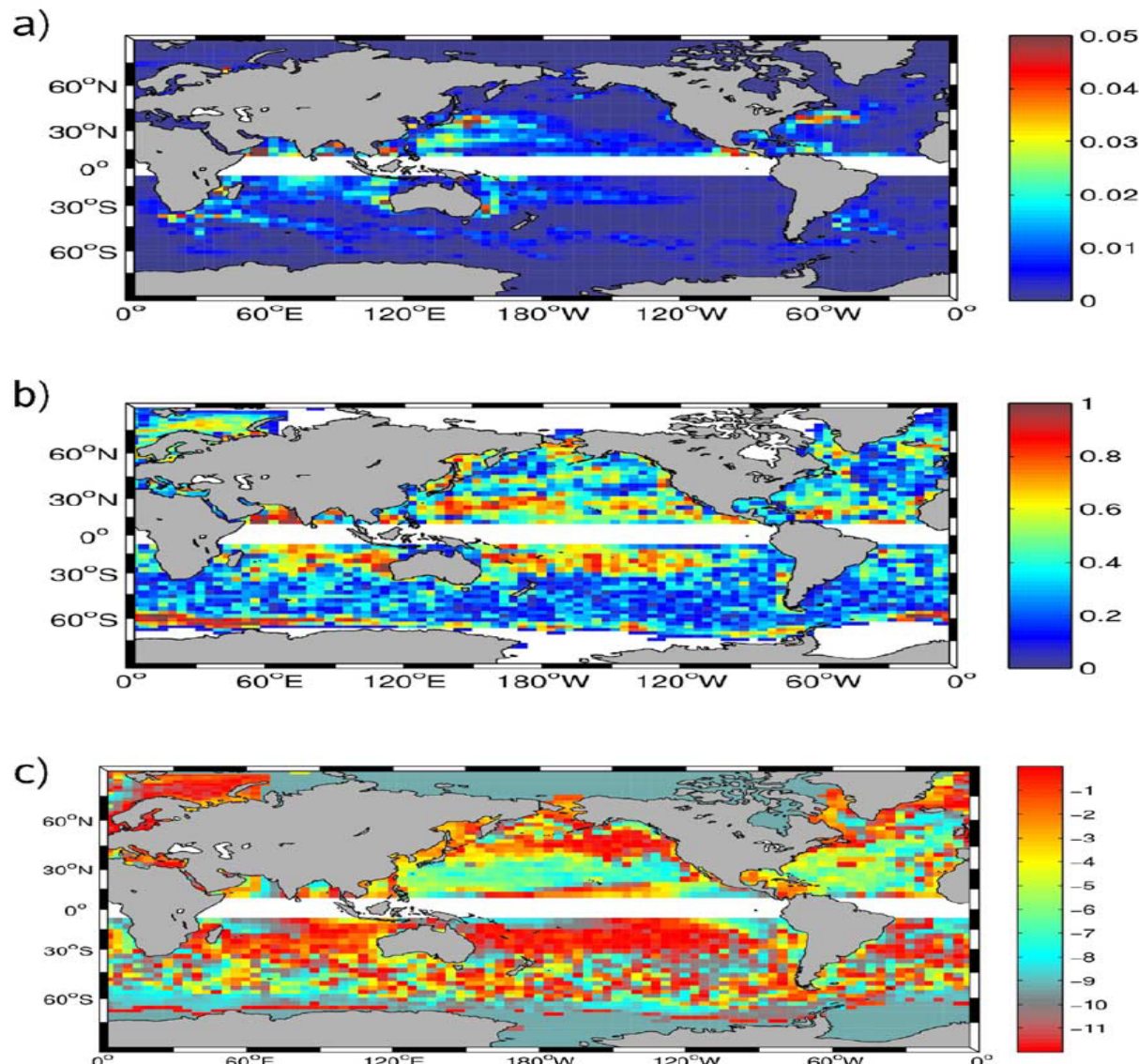


Figure 4. (a) Amplitude of the seasonal cycle of EKE in $m^2 s^{-2}$; (b) amplitude of the seasonal cycle normalized by the total variance; (c) phase of the seasonal cycle relative to January (e.g., -8 means the maximum is in August).

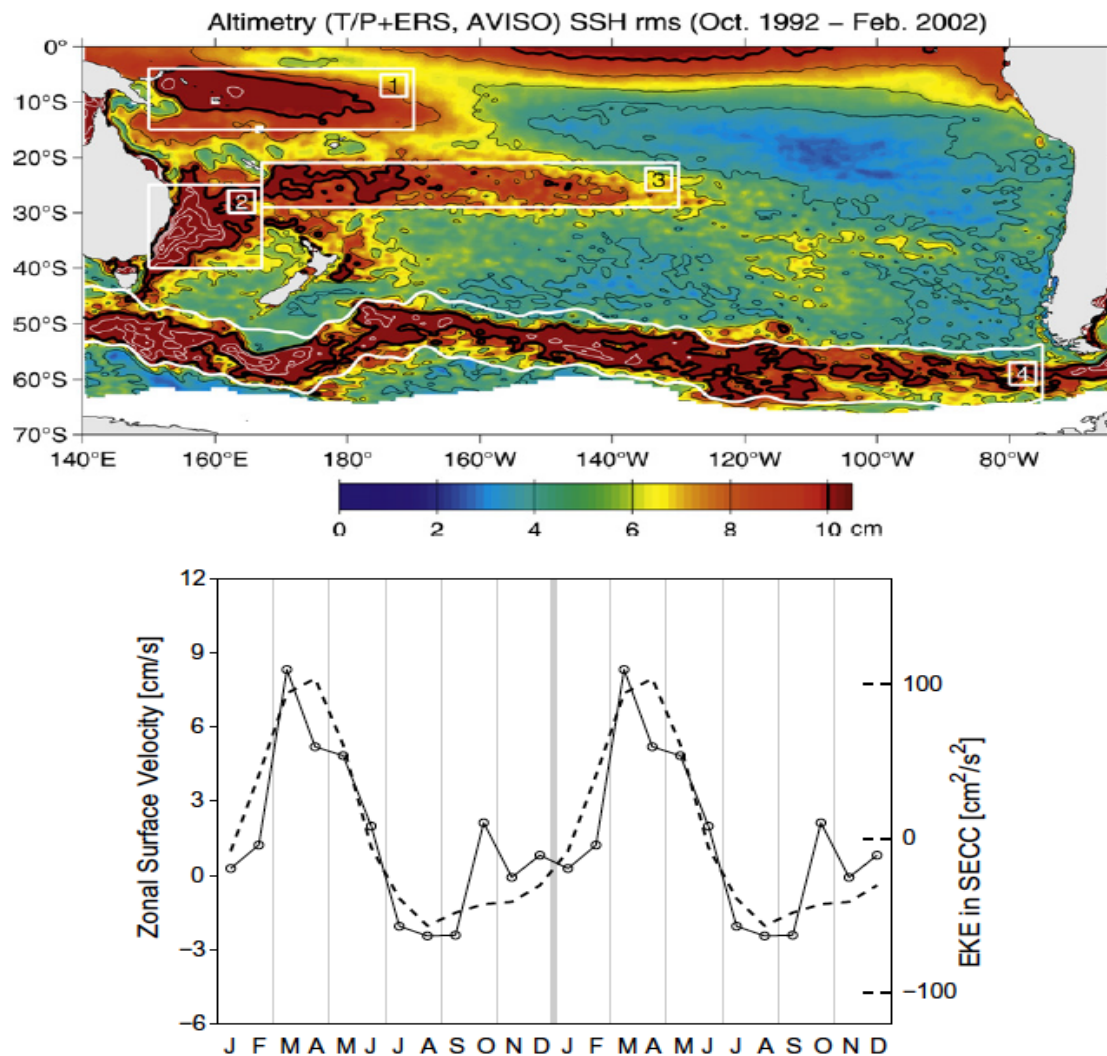


Fig. 3. (a) Map of the rms sea surface height variability from T/P + ERS data in the South Pacific Ocean. Box 1 highlights the SECC variability, Box 3 the STCC variability. (b) Zonal velocity shear between 0 and 600 m for the STCC-SEC from monthly climatological data (solid line) compared to altimeter EKE (dashed line) (after Qiu and Chen, 2004 © American Meteorological Society).